CHAPTER 4
RESULTS AND DISCUSSION

This chapter describes XRD analysis for phase formation of (x)PMN-(1-x)PZT ceramics (when x = 0.0, 0.1, 0.3, 0.5, 0.7, 0.9 and 1.0), including analysis of microstructure of sintered specimens and densification of the materials. Results of polarization versus electric field (P vs. E) measurements made on representative sample, performed to determine the coercive field, hysteresis and polarization achievable are presented.

4.1. Phase formation analysis

XRD analysis was performed on sintered ceramics to obtain XRD patterns of (x)PMN-(1-x)PZT ceramics as a function of PMN content at room temperature. XRD pattern of PZT ceramic is shown in figure 4.1, which could be matched with JCPDS file no. 50-346, indicating a tetragonal structure in space group P4mm (no. 99) with lattice parameters a = 4.017 Å and c = 4.139 Å.[45] Perovskite phase appears to have a tetragonal symmetry for $Pb(Zr_{0.44}Ti_{0.56})O_3$ ceramic. This is probably due to a combination of the carefully optimized reaction to form single phase precursor powders and the refined sintering procedure.

Figure 4.2 shows XRD pattern of PMN ceramic, which could be matched with JCPDS file no. 27-1199, indicationg a cubic perovskite-type structure in space group Pm3m (no. 221) with lattice parameters a = 4.049 Å.[43] However, a small amount of pyrochlore phase of $Pb_{1.83}Nb_{1.71}Mg_{0.29}O_{6.39}$ could be matched with JCPDS file no. 33-769 with a cubic structure and lattice parameter a = 10.59 Å in space group Fd3m (no. 227).[43, 45] The relative amounts of perovskite and pyrochlore phases were determined from XRD patterns of the sample by measuring the major peak intensities for the perovskite (110) and pyrochlore (222) phases. The following qualitative equation was used,[42]

$$\%\,perovskite = \frac{100\,\upsilon\,(I_{110})_{perovskite}}{(I_{110})_{perovskite} + (I_{222})_{pyrochlore}}$$

It is calculated that the volume fraction of the perovskite phase is 94% for PMN ceramic. The small amount of pyrochlore formed in PMN ceramic could be attributed to many factors, including inhomogeneity of the mixture,[46] a slight magnesium deficiency caused by the presence of volatile substances in the as received MgO powder and PbO-loss during sintering process.[47, 48, 49, 50]

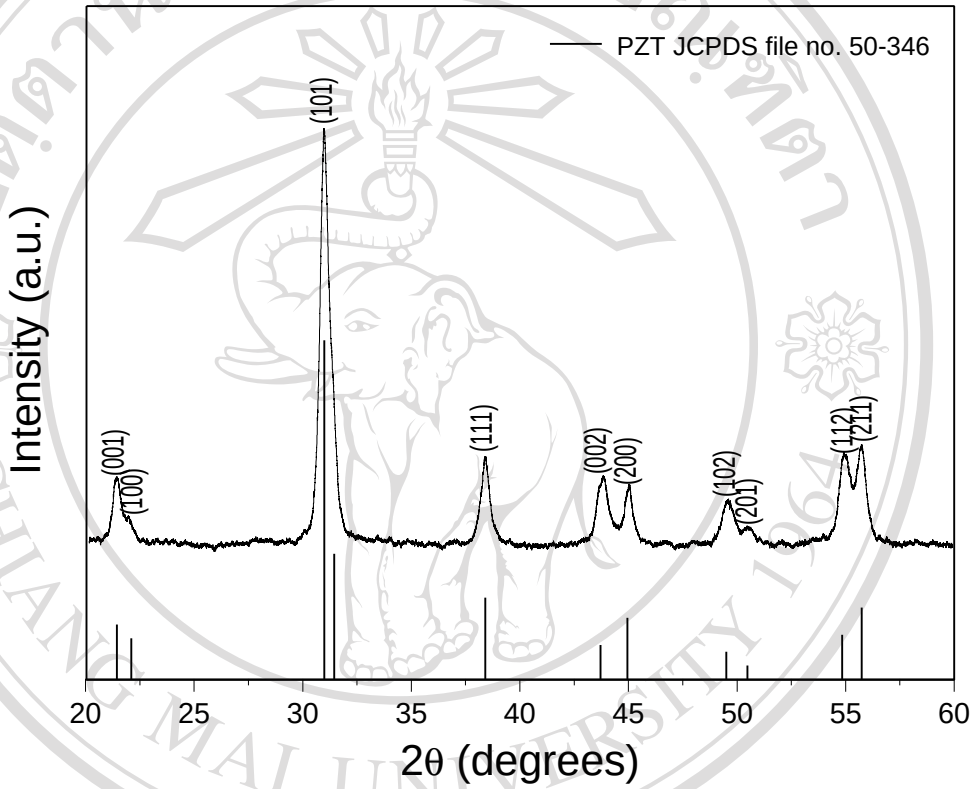

Figure 4.1 XRD pattern of PZT ceramic (with JCPDS file no. 50-346)

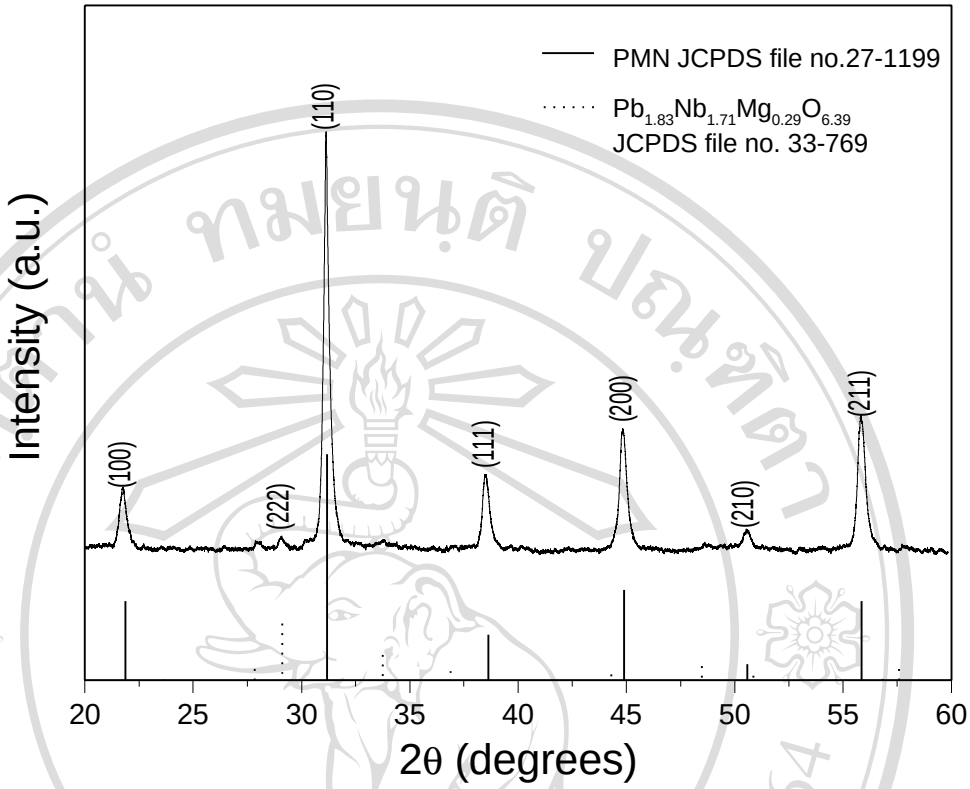

Figure 4.2 XRD pattern of PMN ceramic (with JCPDS file no. 27-1199) including small amount of pyrochlore (with JCPDS file no. 33-769)

XRD patterns of (x)PMN-(1-x)PZT ceramics with various x values are shown in figure 4.3. The XRD patterns, which were obtained for sintered ceramics with maximum density, show that a complete crystalline of perovskite structure was formed throughout the whole composition ranges. For the compositions with x values between 0.1 and 0.9, no pyrochlore phase has been detected. The small quantity of pyrochlore phase presence in PMN was eliminated from the composites of PMN and PZT. The PZT phase apparently acted as a seed for the PMN and transformed the composite to perovskite phase only.[51] The XRD patterns of the composites show a combination between PMN and PZT patterns. Morphotropic compositions between x = 0.3 and x = 0.5 exhibited the peak splits into two reflections. These features are obviously associated with the samples, in which two or more phases coexist.

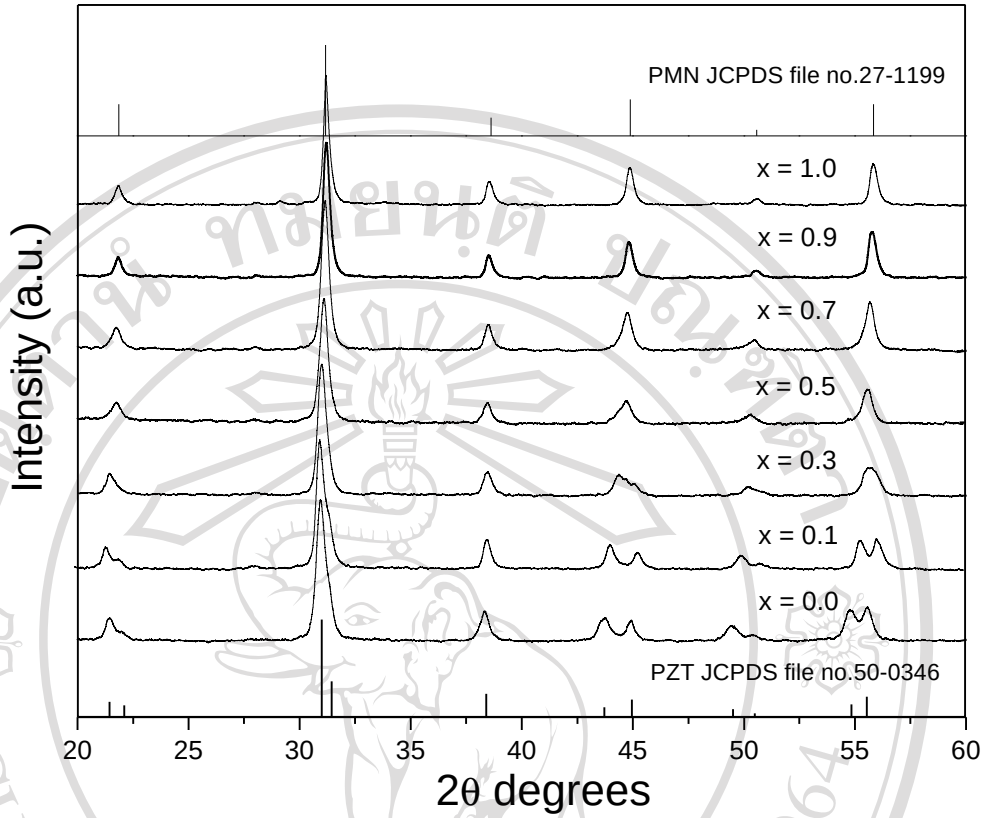

Figure 4.3 XRD patterns of (x)PMN-(1-x)PZT ceramics

4.2. Microstructural analysis

Microstructures were analyzed both at free and fracture surfaces of (x)PMN-(1-x)PZT ceramics by scanning electron microscopy (SEM). The ceramics with a maximum density for each composition were chosen for SEM analysis. SEM micrographs show that the grain size of the ceramics varies considerably from < 1 μm to 10 μm, as tabulated in Table 4.1. However average sizes of the ceramics do not vary significantly with composition. The average grain size could be qualitatively by obtained by using line intercept method.[52]

SEM micrographs also show pores at grain boundaries, intragrains (close pore) and crack. The micrographs reveal that the PMN modification increases degrees of grain close packing. It should be noted that some of the grains are observed to be in irregular shapes with some open pores. The ZrO_2 are found in PZT ceramic (as see in figure 4.4) which result of In figures 4.5 to 4.7 (for (x)PMN-(1-x)PZT when x = 0.1, 0.3, 0.5), abnormal grain growth and melting zone can be seen, probably a result of over sintering temperature for each ceramic. Many open pores on the surface of ceramic with x = 0.3 can be observed, as a result of a high rate of evaporation of PbO

during sintering process.[53] The compositions of x = 0.7, 0.9 and 1.0 show more uniform microstructure with small amount of porosity than other compositions. The pyrochlore grains were also found on free surface of PMN ceramics. Two types of grains with different morphology can be observed in these ceramics. These specimens contained the rounded $Pb(Mg_{0.33}Nb_{0.67})O_3$ grains and the polyhedral pyrochlore grains.[54] The pyrochlore grains were on the surface of the ceramics, a result of a liquid phase sintering mechanism promoted by an excess of PbO.[46] The formation of the liquid phase during sintering can be attributed to PbO as well as the weight loss, since the PbO melting point (889 °C) is lower than that of other components (MgO, Nb_2O_5, $MgNb_2O_6$, m.p.>1100 °C).[47] This phase promotes a liquid phase sintering process that decreases the densification temperature but at the same time undergoes PbO volatilization with subsequent formation of pyrochlore.[55] In PMN-PZT composite micrographs, the grains with submicron size were found on surfaces of larger grains and grain boundaries (as seen in figures 4.5 to 4.10). In figures 4.11 and 4.12, the EDS analysis reveals that the submicron size grains and larger grain correspond to PMN-PZT compound with no compositional difference existing between the submicron size grains and the larger grain. It is possible to note that during sintering process, there is disintegration of some particles.[56]

Table 4.1 Grain size range of (x)PMN-(1-x)PZT ceramics

Ceramics	Grain size range (μm)
PZT	1-6
0.1PMN-0.9PZT	0.5-3
0.3PMN-0.7PZT	1-6
0.5PMN-0.5PZT	0.1-7
0.7PMN-0.3PZT	1-5
0.9PMN-0.1PZT	2-10
PMN	1-8

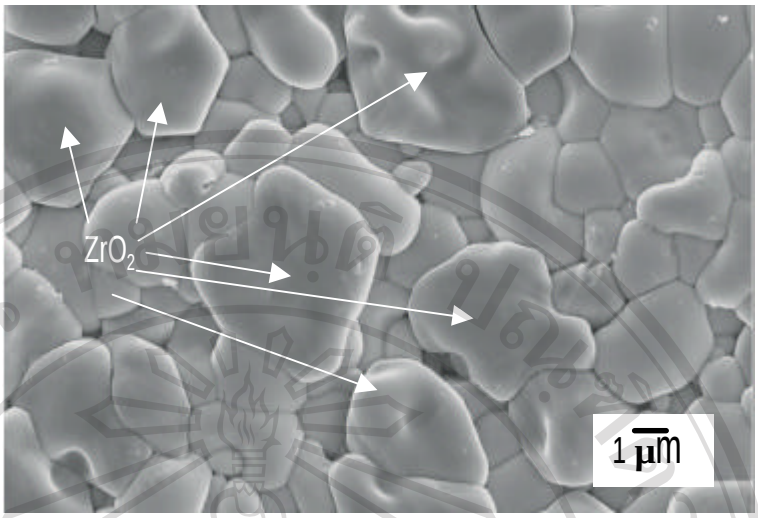

(a)

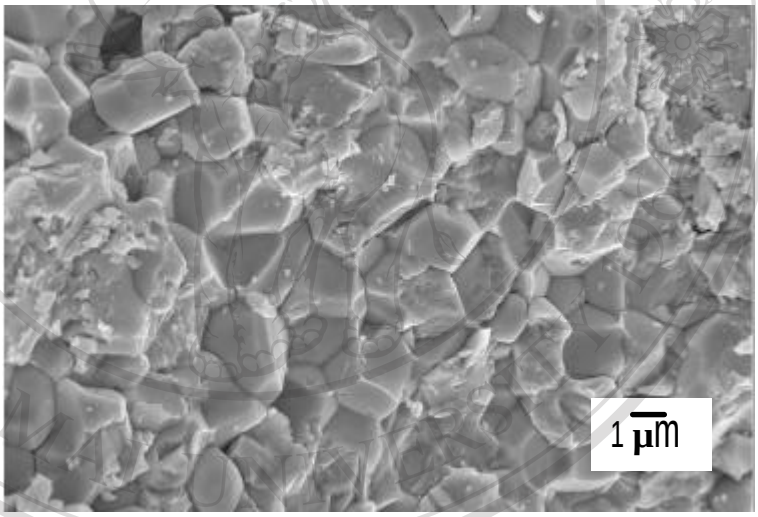

(b)

Figure 4.4 SEM micrograph of (a) free and (b) fracture surfaces of PZT ceramic

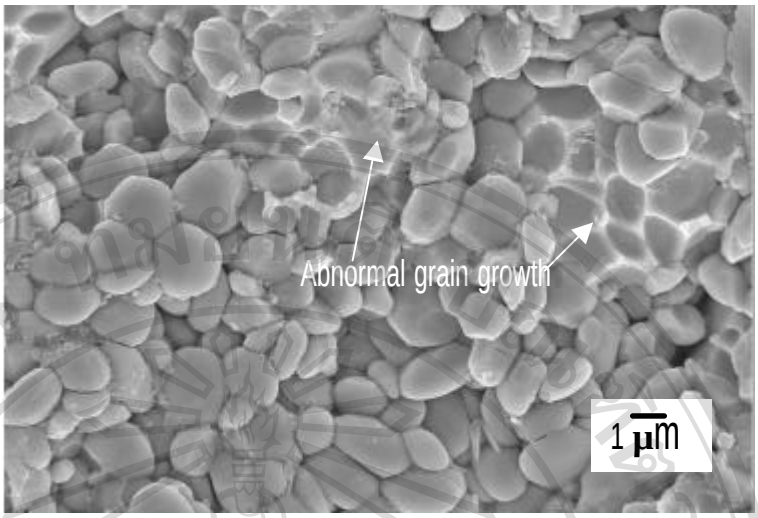

(a)

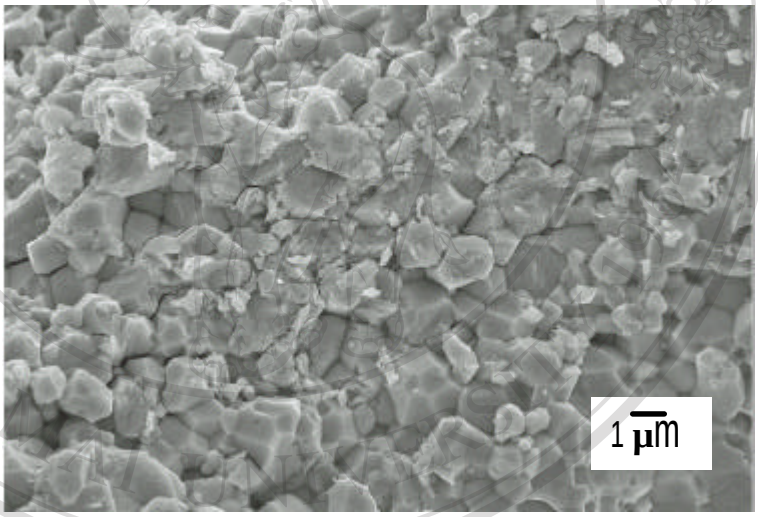

(b)

Figure 4.5 SEM micrograph of (a) free and (b) fracture surfaces of (0.1)PMN-(0.9)PZT ceramic

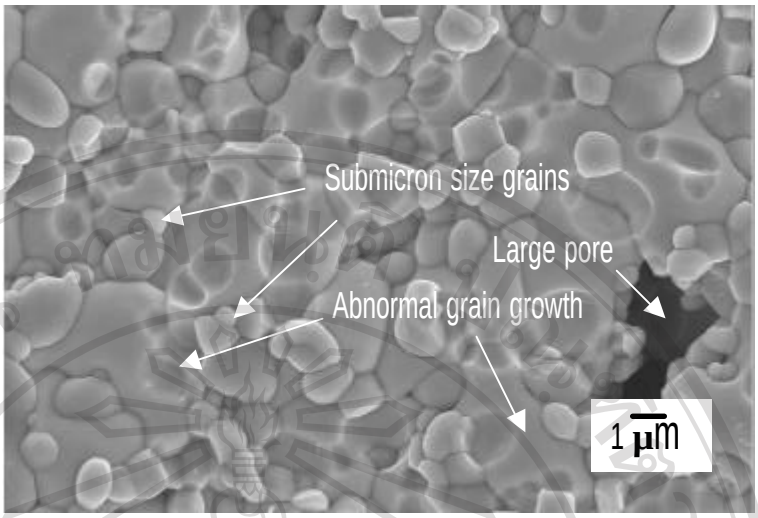

(a)

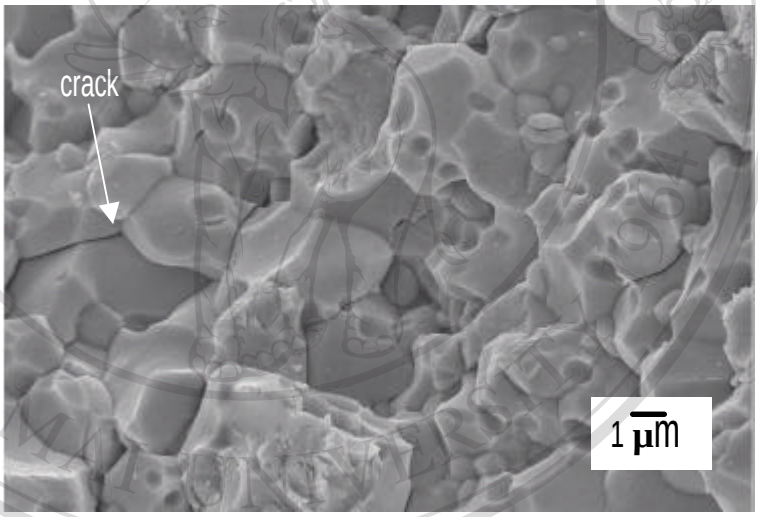

(b)

Figure 4.6 SEM micrograph of (a) free and (b) fracture surfaces of (0.3)PMN-(0.7)PZT ceramic

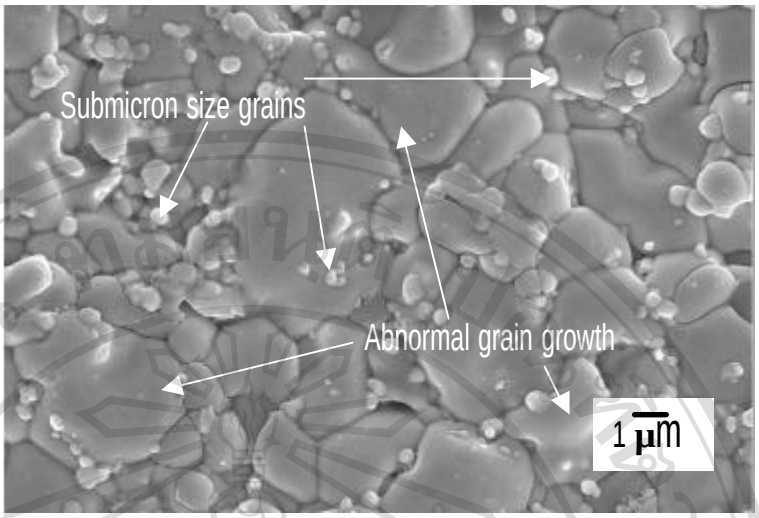

(a)

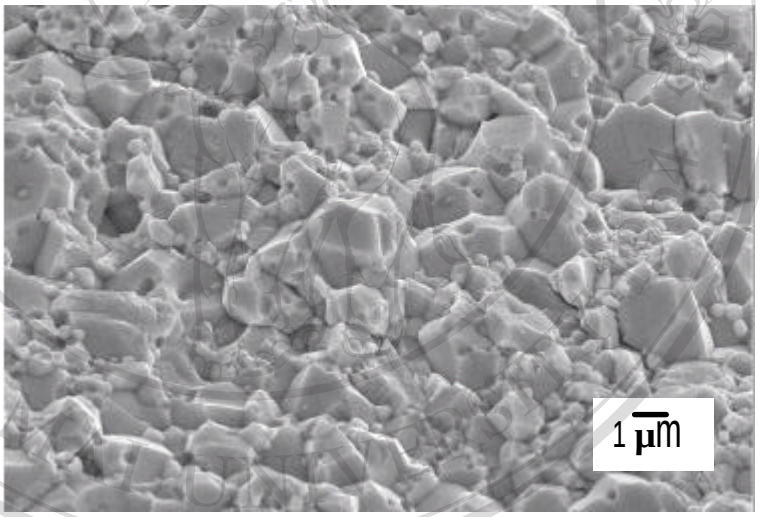

(b)

Figure 4.7 SEM micrograph of (a) free and (b) fracture surfaces of (0.5)PMN-(0.5)PZT ceramic

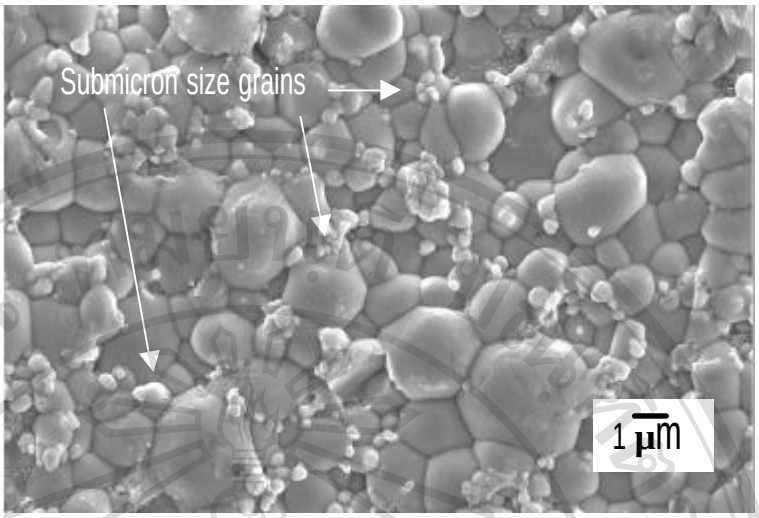

(a)

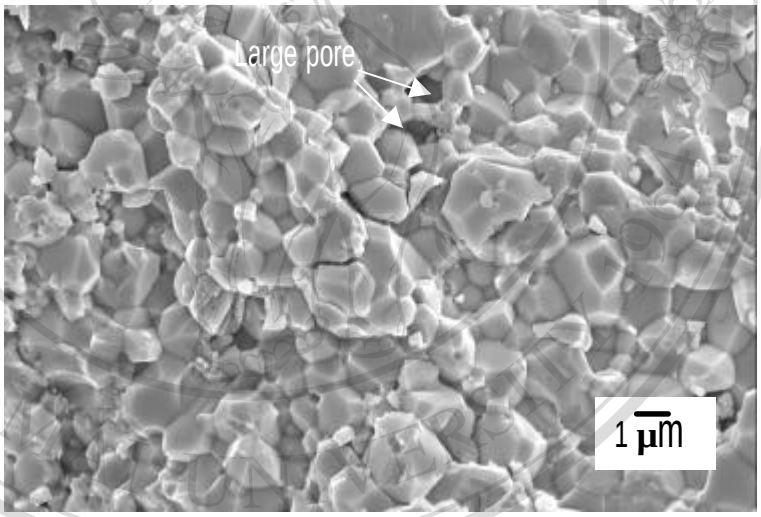

(b)

Figure 4.8 SEM micrograph of (a) free and (b) fracture surfaces of (0.7)PMN-(0.3)PZT ceramic

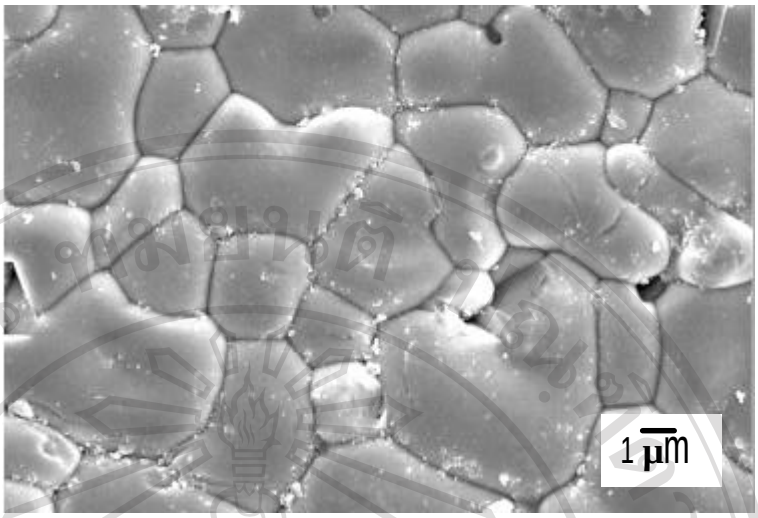

(a)

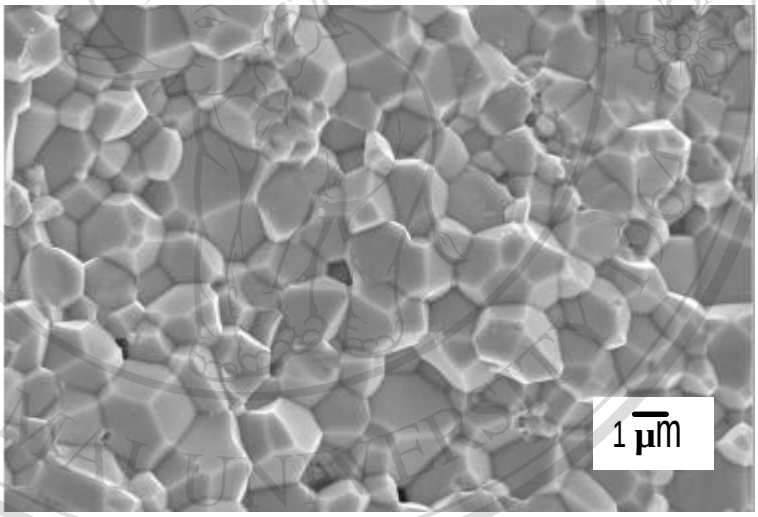

(b)

Figure 4.9 SEM micrograph of (a) free and (b) fracture surfaces of (0.9)PMN-(0.1)PZT ceramic

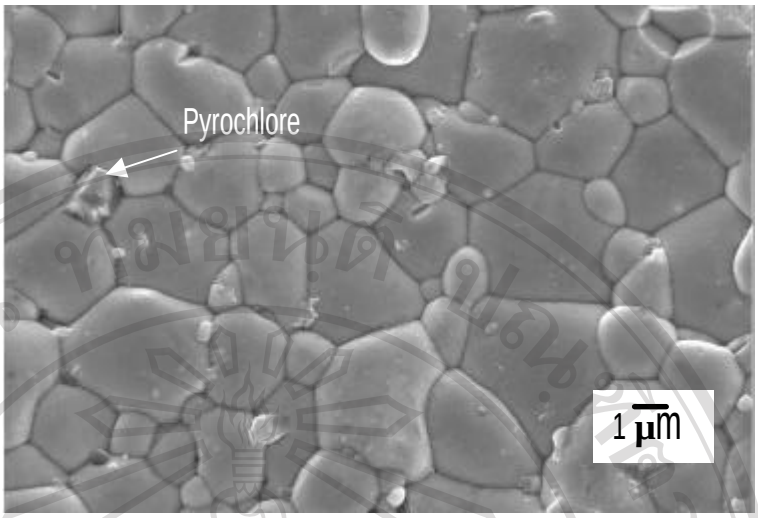

(a)

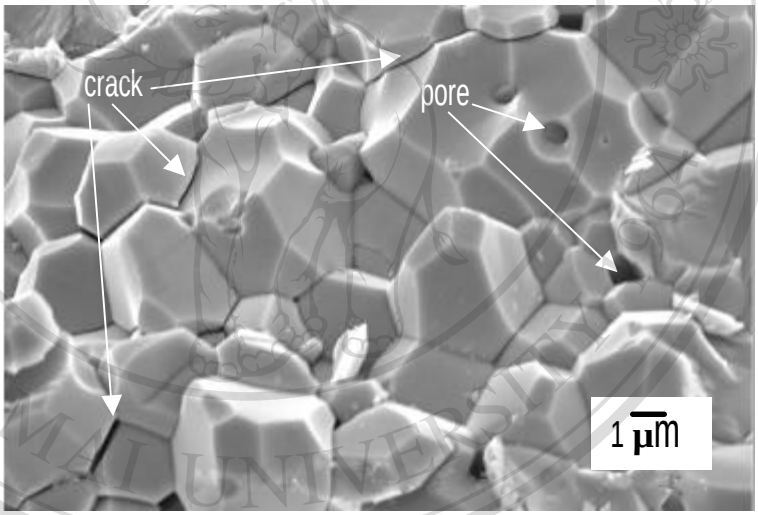

(b)

Figure 4.10 SEM micrograph of (a) free and (b) fracture surfaces of PMN ceramic

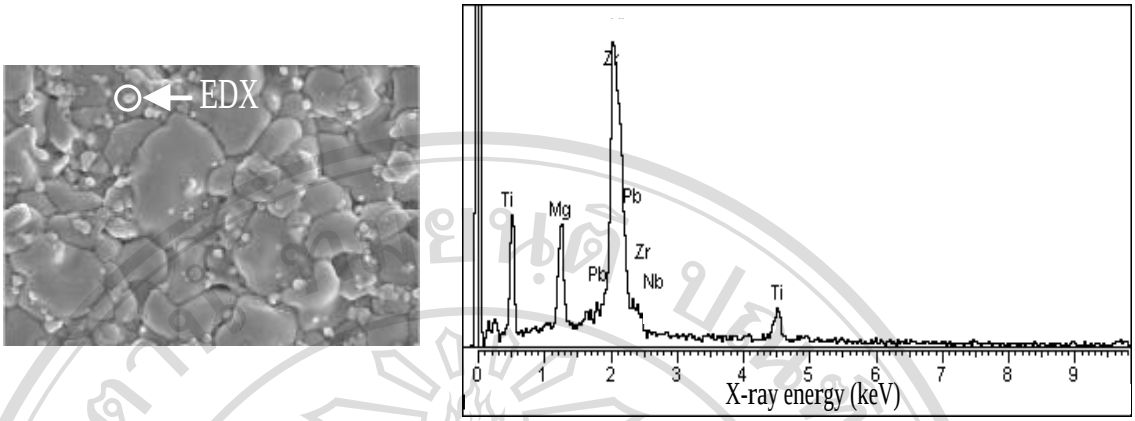

Figure 4.11 Representative EDX spectra obtained from submicron size grains on the surface of (x)PMN-(1-x)PZT ceramics

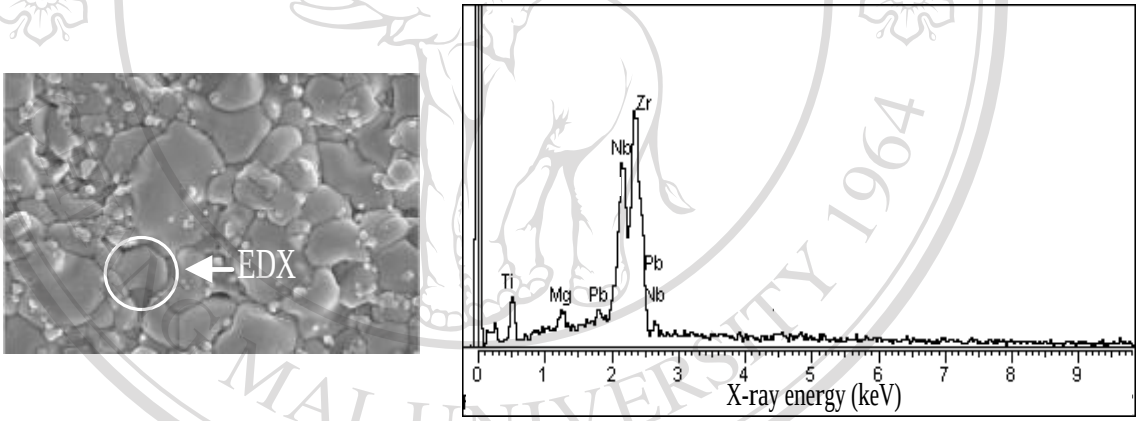

Figure 4.12 Representative EDX spectra obtained from large grain on the surface of 0.5PMN-0.5PZT ceramics

4.3. Densification analysis

The density was measured after sintering for representative samples of all compositions investigated to insure reproducibility in subsequent electrical property measurements. Sintered densities are obtained and presented in figure 4.13. It is found that the density of PMN is 96.9% of theoretical density, while the density of PZT is 96.7% of theoretical density. Moreover, it is observed that the density of ceramics is composition-independent. By comparison, 0.9PMN-0.1PZT ceramic has a maximum density of 8.01 g/cm^3 while 0.5PMN-0.5PZT ceramic has a minimum density of 7.34 g/cm^3. It is probably the effect of porosity which occurs in sintering process. These results also correspond to morphology of microstructure as 0.9PMN-0.1PZT ceramic has high degrees of grain close packing microstructure while 0.5PMN-0.5PZT ceramic has many infra grain pores (close pores). The Archimedes principle shows the apparent solid density that is the mass of the solid divided by the apparent solid volume. This consists of the true volume of solid plus the volume of any closed pores that are present. It indicates the error of the Archimedes method. These characteristics influence to the electrical property.[57] However, this shows that the microstructure has significant effect on the density of the ceramics.

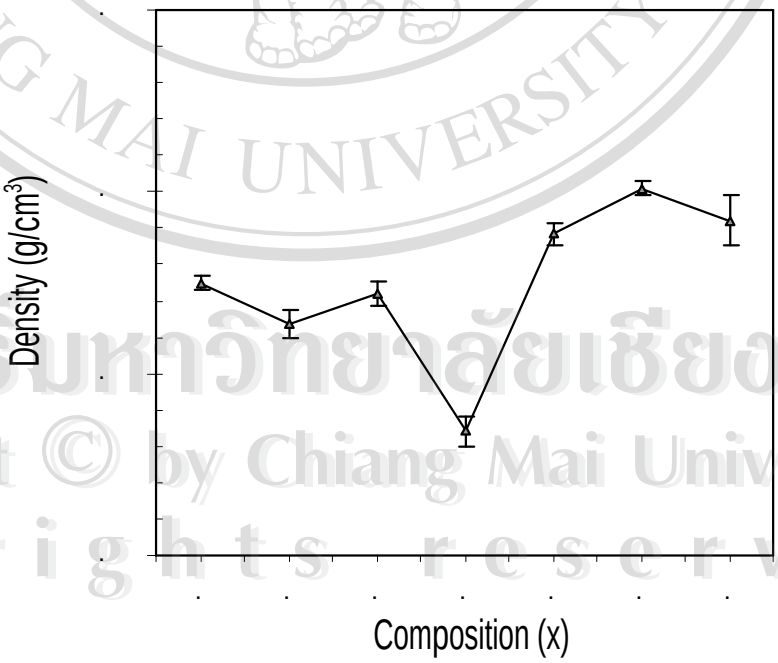

Figure 4.13 Densities of (x)PMN-(1-x)PZT ceramics

4.4. Hysteresis properties

The hysteresis properties of poled samples were measured by a standard Sawyer-Tower circuit (as described in section 3.3). The hysteresis parameters, which are spontaneous polarization (P_s), remanent polarization (P_r) and coercive field (E_c) were determined and then calculated. The hysteresis loop characteristics with varying applied electric field, the hysteresis parameters dependence on composition ratio and poling condition were subsequently studied.

Initially, an experimental setup was calibrated through measurement of hysteresis loop of commercial PZT sample (PKI-552 or soft PZT). Figure 4.14 illustrates hysteresis loop of soft PZT taken at various AC drive amplitudes. The figure clearly demonstrates that the hysteresis loop gradually develops with increasing magnitude of the AC field at a maximum AC field. At an applied field of 19.20 kV/cm, the values of remanent polarization (P_r), spontaneous polarization (P_s) and coercive field (E_c) were found to be about 24.83 $\mu C/cm^2$, 26.48 $\mu C/cm^2$ and 6.76 kV/cm, respectively. These values of soft PZT determined in this experiment are close to those of other researches.[58,59] These clearly show that the set-up is fairly accurate and reliable.

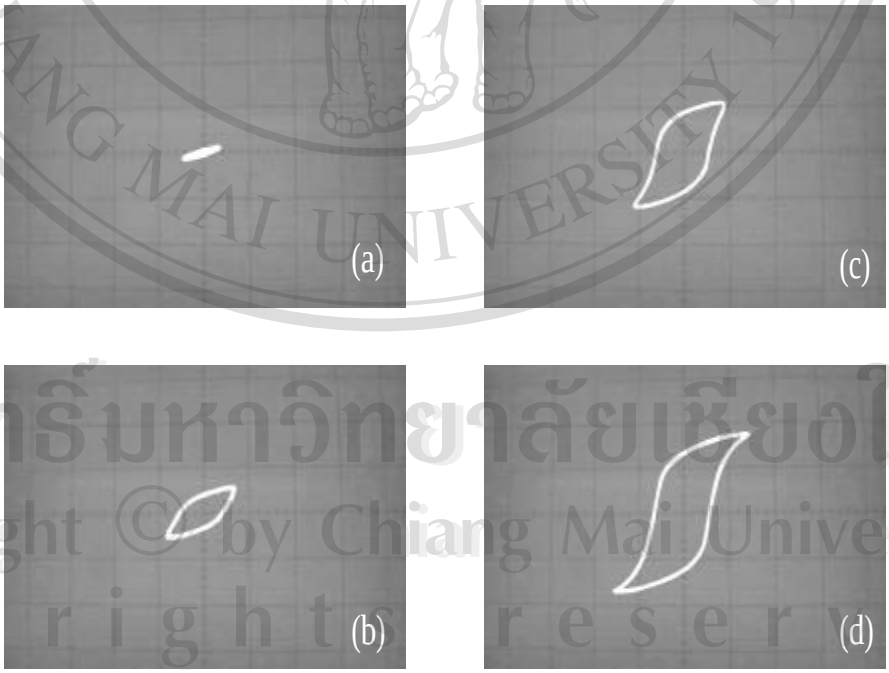

Figure 4.14 Hysteresis loop evolution of commercial sample (PKI-552 or soft PZT) taken at AC drive amplitudes of: (a) 5.13, (b) 10.14, (c) 12.17 and (d) 19.20 kV/cm

4.4.1. Hysteresis loop evolution

The hysteresis loop features of (x)PMN-(1-x)PZT ceramics were studied at various applied electric field. From figures 4.15 to 4.21, generally, it is found that a straight line appears at low field, however at higher field (at threshold magnitude of AC field) the loops popped open and showed a ferroelectric behavior. These results are due to the most important characteristic of ferroelectric materials, which is a polarization reversal (or switching) by an external electric field.[12] Application of the low electric field generates a linear relationship between P and E because the field is sufficient to switch small portion of domains. As the electric field strength increases, a number of the domains with opposite polarization direction switch towards the field direction. Finally, the saturated hysteresis loops occur when all the domains are aligned as well as possible in the field direction and a saturation state is reached. The following contents show the hysteresis loop evolution under AC field of each composition of (x)PMN-(1-x)PZT ceramics which poled at 30 kV/cm of DC poling field. The hysteresis loop evolution of (x)PMN-(1-x)PZT ceramics for other poling condition at 10 to 40 kV/cm of DC poling field are shown in Appendix.

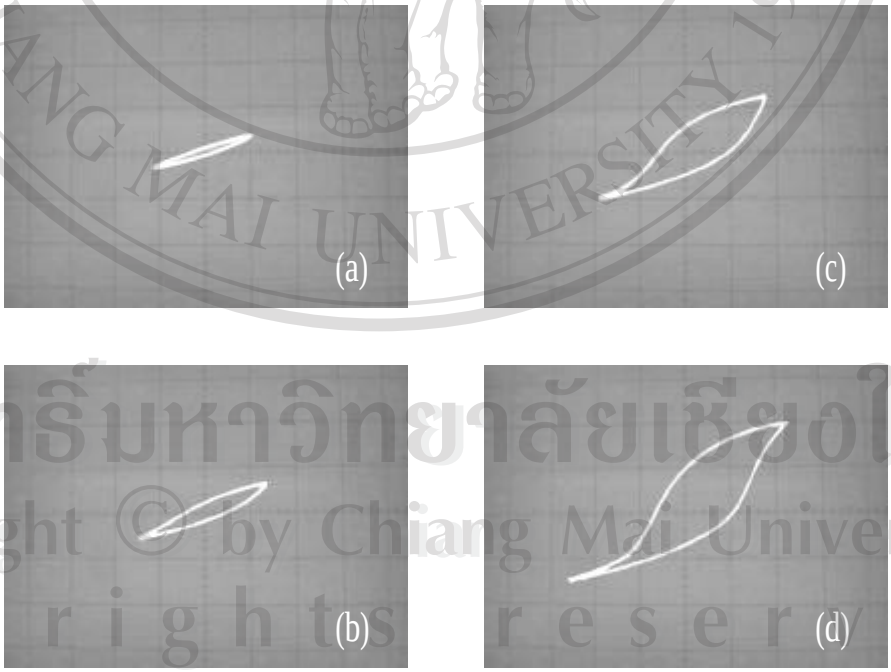

Figure 4.15 Hysteresis loops evolution of PZT ceramics poled at 30 kV/cm taken at AC drive amplitudes of : (a) 6.04, (b) 8.03, (c) 10.09 and (d) 14.06 kV/cm

Figure 4.15 illustrates hysteresis loops of PZT ceramics, taken at various AC drive fields. The ceramics were poled at 30 kV/cm of DC poling field. The figures for other poling conditions at 10 to 30 kV/cm of DC poling field are shown in Appendix. The loop is well-develop with increasing AC applied field. The hysteresis loop of PZT ceramic is a square type. The square form of the loop is stipulated by abruptly switching of a domain structure in an electric field, which is typical for a phase that contains long-range corporation between dipoles.[8,29] This is a characteristic of a ferroelectric macrodomain state. In addition, these figures show a ferroelectric shape (sigmoid shape as seen in figure 4.15(b)) at $E \cong E_c$ (E_c= 7.95 KV/cm), the spontaneous polarization starts reversing. When $E > E_c$, domains align as close as possible to the direction of the applied field and domain boundaries are eliminated. These results are in clear distinction to those expected from a conventional ferroelectric concept.[60] According to conventional ferroelectric concept, polarization switching does not occur until $E > E_c$. Upon application of a field, a near-linear reversible polarization is induced, but returns to zero after removal of the field. No remanent polarization or hysteresis is induced until the coercive field (E_c) is exceeded. At E_c, polarization switching occurs by realignment of domains in the direction of the applied field. As a result of domain realignment, hysteresis is observed.[60]

It is also evident that the width of the loop on a positive sign of the applied AC field is wider than that of the negative sign of the applied AC field. The wider side of the loop needs more energy to switch polarization than the other side. This probably is an effect of pinning which suppresses domain wall motion, including the effect of the poling direction. The domain wall mobility is in large part determined by the interaction with structural imperfections like the outer perimeter of a crystal, grain boundaries, inclusions, point defects or their agglomerates. As a result, the shape of the hysteresis loop is altered.[61] Hence, this reveals asymmetry in P-E loop shape.

Moreover, it is found that the positive coercive field ($+E_c$= 7.95 kV/cm) is larger in absolute value than the negative coercive field ($-E_c$= 6.36 kV/cm). This asymmetry is similar to that previously reported for hard PZT.[62] Such asymmetry is due to the presence of a net built-in internal dipolar field, due to the alignment of the dipolar field of individual defect dipole complexes.[62, 63, 64, 65] Ferroelectric domains are pinned by internal fields, due to defect complexes of impurities such as ZrO_2. Such defect complexes could gradually develop net dipolar field by aligning local dipole moments parallel to the spontaneous polarization.[66]

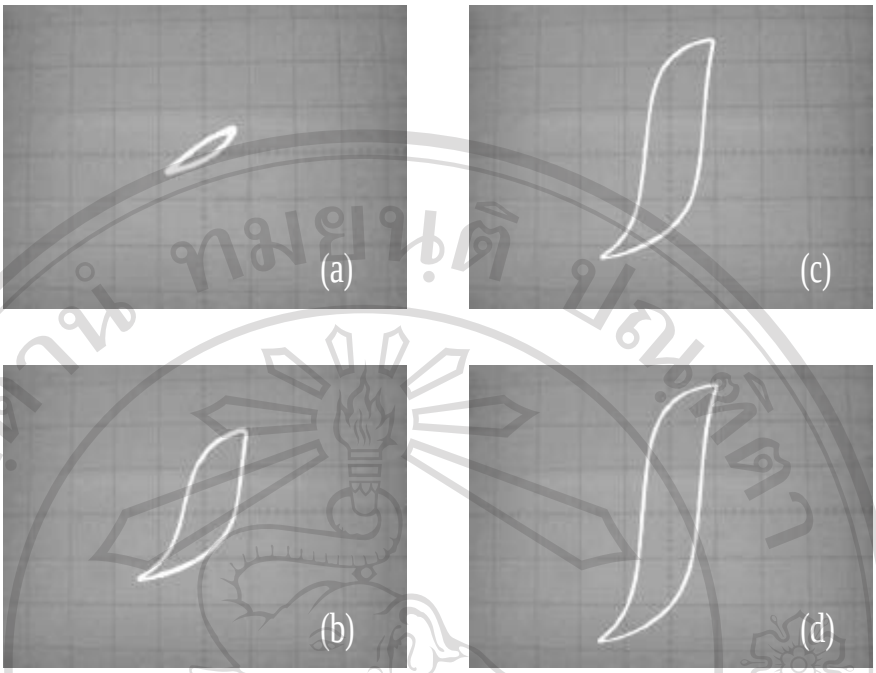

Figure 4.16 Hysteresis loops of 0.1PMN-0.9PZT ceramics poled at 30 kV/cm taken at AC drive amplitudes of : (a) 4.57, (b) 6.03, (c) 9.04 and (d) 11.14 kV/cm

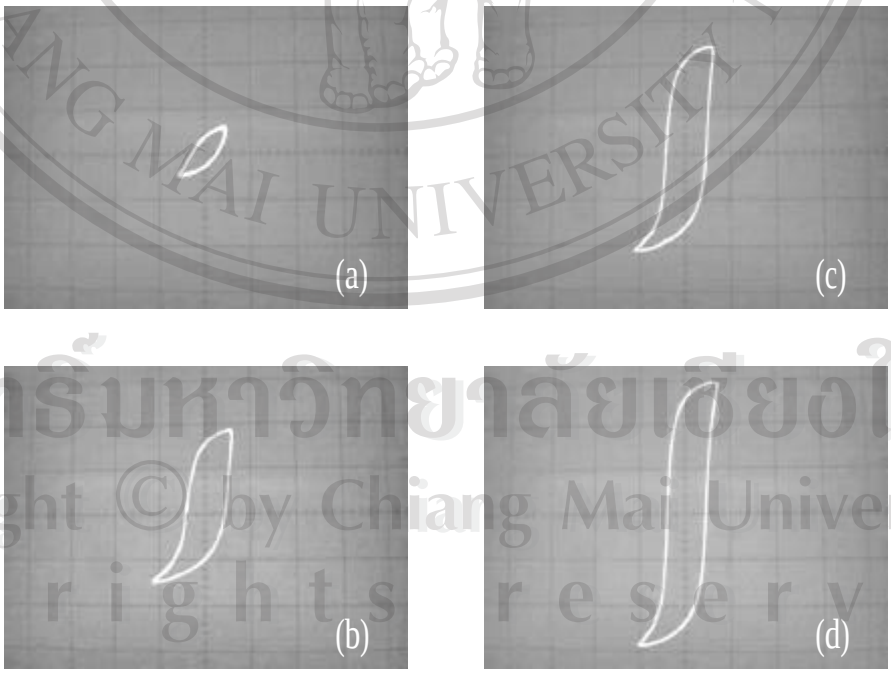

Figure 4.17 Hysteresis loops of 0.3PMN-0.7PZT ceramics poled at 30 kV/cm taken at AC drive amplitudes of : (a) 4.04, (b) 5.04, (c) 6.54 and (d) 8.04 kV/cm

Figures 4.16 and 4.17 show hysteresis loop evolution of 0.1PMN-0.9PZT and 0.3PMN-0.7PZT ceramics, respectively. The saturated loop of 0.1PMN-0.9PZT (as seen in figure 4.16 (d)) is more square than that of 0.3PMN-0.7PZT. However, both loops are still less square than the loop of PZT ceramic (shown in figure 4.15). Furthermore, these loops show the ferroelectric shape for $E > E_c$ and the saturated loops also show asymmetry, a similar characteristic to that of PZT ceramic.

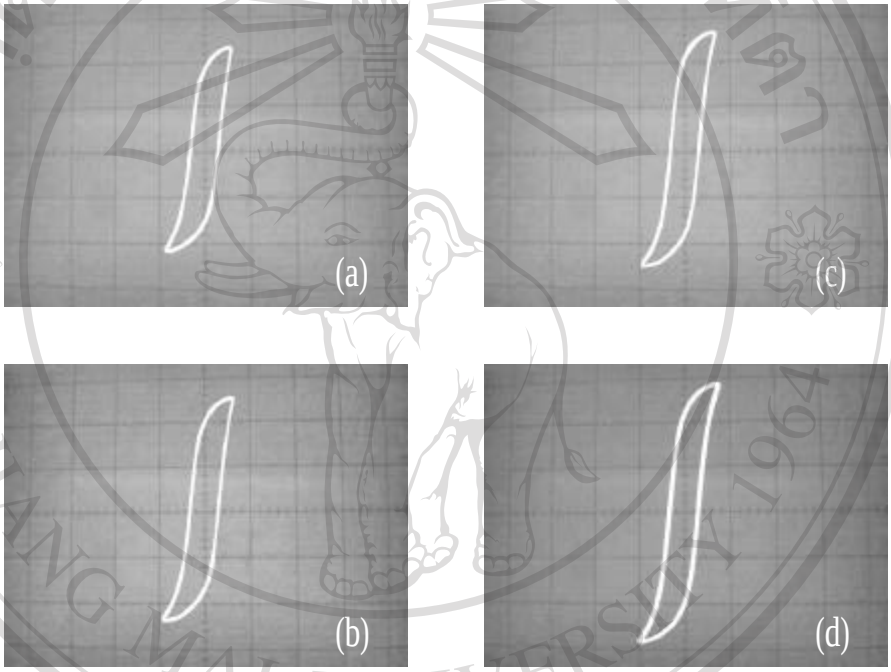

Figure 4.18 Hysteresis loops of 0.5PMN-0.5PZT ceramics poled at 30 kV/cm taken at AC drive amplitudes of : (a) 8.11, (b) 9.12, (c) 9.56 and (d) 10.13 kV/cm

The hysteresis loop evolution of 0.5PMN-0.5PZT ceramic poled at 30 kV/cm is shown in figure 4.18. It illustrates fairly stable shapes with increasing AC applied field. Moreover, they are slimmer than those of previous compositions.

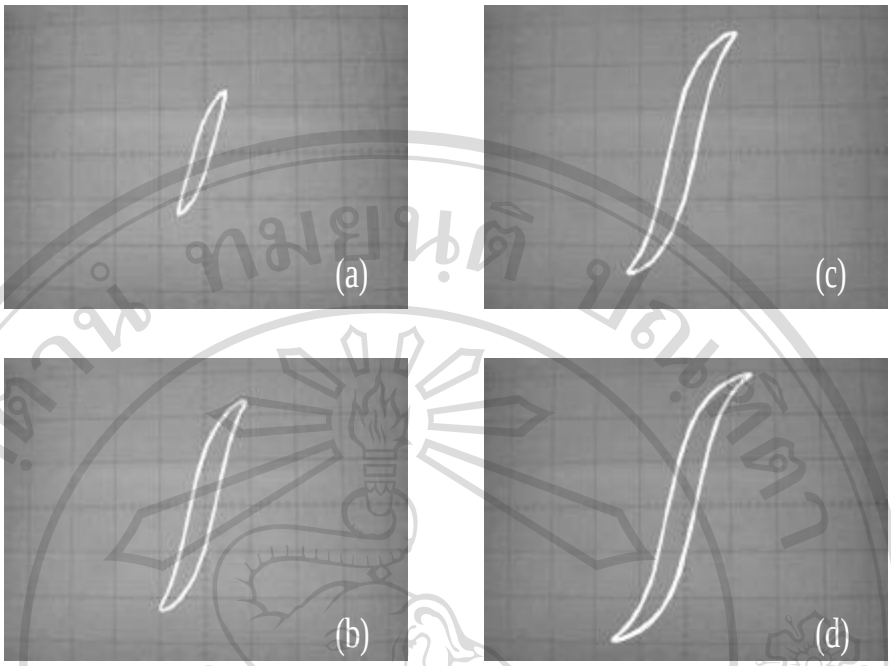

Figure 4.19 Hysteresis loops of 0.7PMN-0.3PZT ceramics poled at 30 kV/cm taken at AC drive amplitudes of : (a) 6.05, (b) 11.03, (c) 14.00 and (d) 18.03 kV/cm

The hysteresis loop evolution of 0.7PMN-0.3PZT ceramic poled at 30 kV/cm is shown in figure 4.19. It is evident that fairly symmetric hysteresis loops with the field are obtained. In addition, the loop evolution is significantly polarization switching does not occur until $E > E_c$. At $E = E_c$, the ferroelectric shape does not appear for 0.7PMN-0.3PZT because a linear reversible polarization is induced. The hysteresis loop arises well over $E >> E_c$. These results are the effect of long-range polar order, which does not develop on this composition, rather relaxor-like ferroelectric characteristics are observed. The characteristics of a relaxor state are often cited polar cluster or microdomain.[67]

The hysteresis loop evolution of 0.9PMN-0.1PZT ceramics poled at 30 kV/cm is shown in figure 4.20. Generally, the loops are well-developed and are fairly symmetric with the field. Hysteresis loops of 0.9PMN-0.1PZT ceramics are less square than those of previously cited compositions. Similar hysteresis loop characteristic is found for PMN ceramic (shown in figure 4.21). The hysteresis loop of PMN shows a slim form type owing to more sluggish reversal. Slim loop exhibits a slight ferroelectricity at room temperature and is typical of a phase with a suppressed long-range interaction of macrodomain. Clearly, the loop of PMN shows a characteristic of a long-range ferroelectric domain state, and is typical of a relaxor ferroelectric.[8]

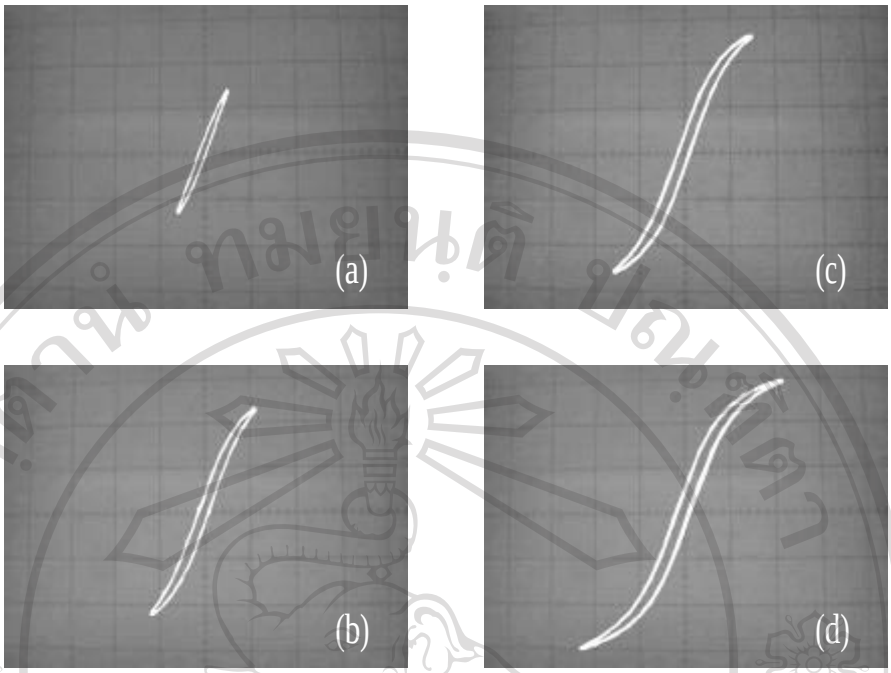

Figure 4.20 Hysteresis loops of 0.9PMN-0.1PZT ceramics poled at 30 kV/cm taken at AC drive amplitudes of : (a) 5.59, (b) 11.08, (c) 15.03 and (d) 20.03 kV/cm

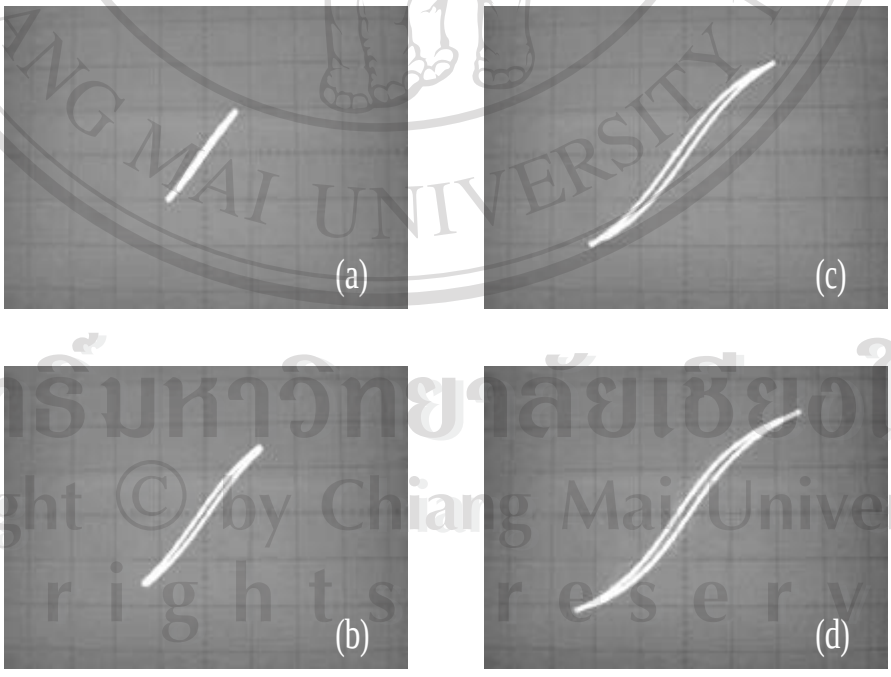

Figure 4.21 Hysteresis loops of PMN ceramics poled at 30 kV/cm taken at AC drive amplitudes of : (a) 6.04, (b) 7.05, (c) 15.03 and (d) 20.14 kV/cm

The hysteresis loop characteristics of (x)PMN-(1-x)PZT ceramics (when $0 \leq x \leq 1$) are illustrated in the preceeding section. It is shown that the squareness of hysteresis loop depends greatly on the PMN content. The hysteresis loops obtained in this experiment are distinguished into two types: square loops and slim loops. Generally, the saturated loops of PZT-riches compositions (when $0 \leq x \leq 0.3$) are more of a square form. The square form of the loop is stipulated by abruptly switching of a macrodomain in an electric field. Hence, phase of PZT-riched compositions is confirmed to be a normal ferroelectric. On the other hand, the PMN-riched compositions (when $0.5 \leq x \leq 1$) exhibit a slim form which is owing to more sluggish reversal. These results are typical of a phase with a suppressed long-range of interaction of macrodomain. This is a characteristic of slight of a long-range ferroelectric domain state and is typical of a relaxor ferroelectric. It implies the coexistence of macro and micro ferroelectric domains in PMN-riched compositions.

Furthermore, the hysteresis loops of PZT-riched compositions are well-developed and show asymmetry with the field, whereas those of PMN-riched compositions are also well-developed, but are fairly symmetric with the field.

Finally, the hysteresis loop evolution of PZT-riched compositions are according to the conventional ferroelectric concept, in which polarization switching occurs at $E = E_c$, whereas that of the PMN-riched compositions does not follow the concept. In this case the significant polarization switching does not occur until $E >> E_c$.

4.4.2. Hysteresis properties dependence on poling field strength

This section describes the hysteresis properties dependence on poling field strength. The saturated loops were obtained for each ceramic composition poled at different poling fields varying between 10 to 40 kV/cm. The hysteresis parameters (P_r, P_s and E_c) are then determined as a function of the poling field strength. Results are presented for each composition. In general, it is clearly evident that the poling field strength shows different effects on each composition.

4.4.2.1. PZT

The sintered ceramics of PZT were poled at various poling field strengths of 10-30 kV/cm. It is found that the PZT ceramics breakdown at poling field strength of 40 kV/cm. Figure 4.22 shows the saturated loops of PZT samples with different poling field strengths.

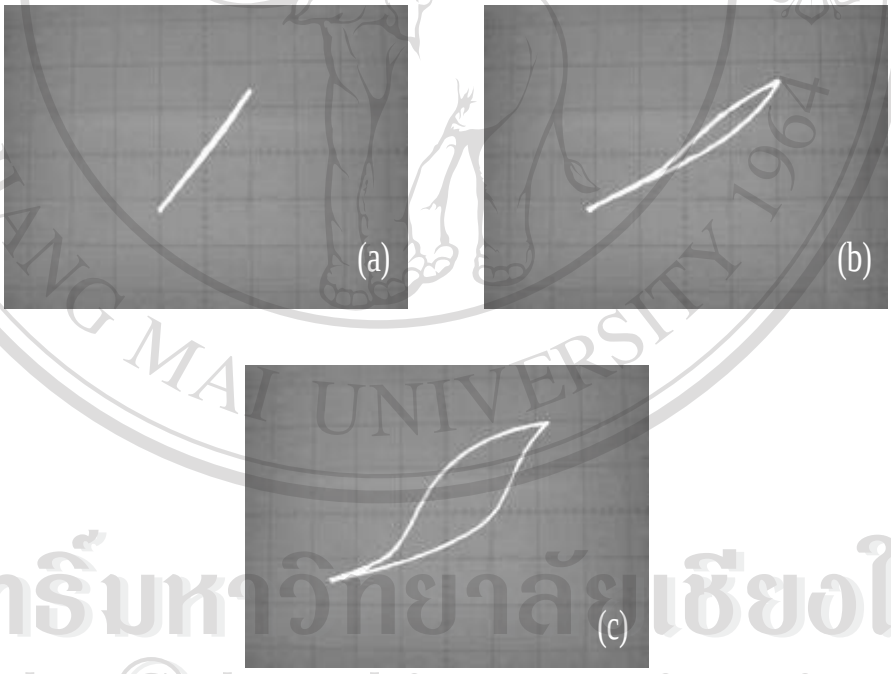

Figure 4.22 The saturated hysteresis loop of PZT ceramics poled at poling field strength of : (a) 10, (b) 20 and (c) 30 kV/cm

It is clearly evident that the shape of hysteresis loops varies greatly with poling field strength. At 10 kV/cm poling field strength, a near-linear relationship of P-E is illustrated in figure 4.22(a). This result is due to the fact that the poling field strength of 10 kV/cm is not large enough to switch any domains. At 20 kV/cm poling field strength (as seen in figure 4.22(b)), polarization nonlinearity is developed in the region of the positive field whereas a linear regime still exhibits in the negative field. These results clearly demonstrate that the poling field strength of 20 kV/cm is of enough energy to constrain realignment of some domains in direction of the applied positive field whereas the negative field is suppressed by pinning.[64] Figure 4.22(c) shows the P-E response for sample poled at 30 kV/cm. The figure reveals fully developed asymmetric hysteresis loop. This shows that the poling field strength of 30 kV/cm is of enough energy to constrain realignment of all domains in direction of the applied field.

The hysteresis parameters (P_r, P_s and E_c) are determined as a function of the poling field strength. The polarization (P_r and P_s) and coercive field (E_c) data as a function of poling field strength for PZT ceramic are listed in Table 4.2, and plotted for better composition in figure 4.23.

Table 4.2 Remanent polarization (P_r), spontaneous polarization (P_s) and coercive field (E_c) of PZT ceramics

Poling field strength	P_r ($\mu C/cm^2$)	P_s ($\mu C/cm^2$)	E_c (kV/cm)
10 kV/cm	0.82	1.68	0.79
20 kV/cm	0.00	2.53	4.77
30 kV/cm	10.10	23.58	7.95
40 kV/cm	Break down	Break down	Break down

From figure 4.23, the coercive field is significantly increased with increasing of poling field strength. These results are due to increasing in magnitude of poling field which in turn makes domains with the polarization direction favorably oriented with respect to the field direction grow at the expense of other domains. The domain polarizations are reoriented to give a new value (or direction) of P_r. Therefore, the increasing of poling field strength induces increasing of remanent polarization. As a result, the coercive field which is the electric field required to switch the polarization from $P = P_r$ to $P = 0$ increases with increment of remanent

polarization.[12] That is, the coercive field increases as a function of the rate of polarization reversal. Furthermore, the spontaneous polarization (P_s) tends to increase with increasing of poling field strength, while the remanent polarization reduces in the initial region of the poling field, then increases abruptly later. These results are a result of an asymmetric loop observed in sample poled at 20 kV/cm, as well as the fact that this poling field does not provide enough energy to realign the domains.

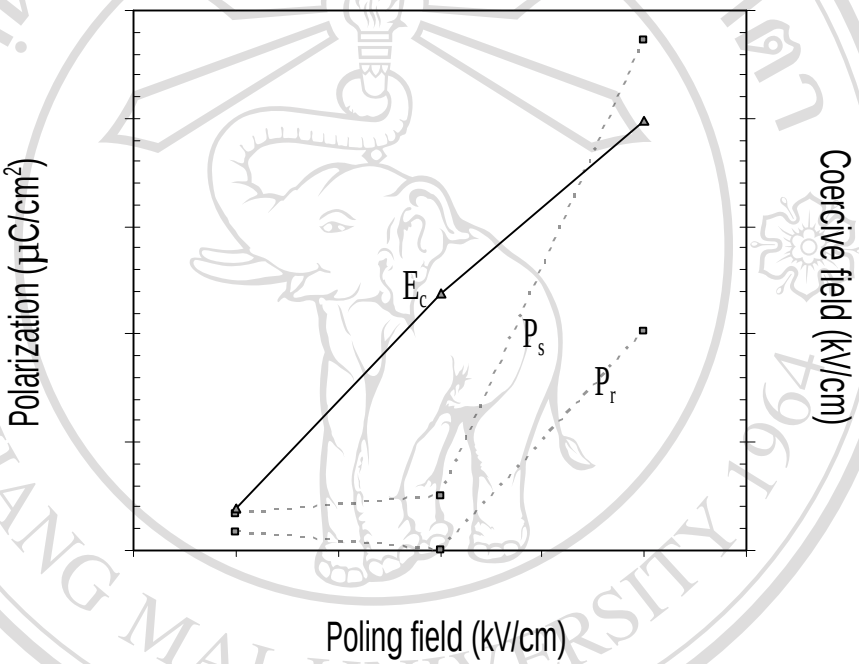

Figure 4.23 The remanent polarization (P_r), spontaneous polarization (P_s) and coercive field (E_c) of PZT ceramic as a function of poling field strength

4.4.2.2. 0.1PMN-0.9PZT

Fully developed hysteresis loops of 0.1PMN-0.9PZT ceramics which were poled between 10 and 40 kV/cm are shown in figure 4.24. In this case, the hysteresis loop shapes are found to be fairly stable even after several poling conditions. However, fairly noticeable changes of the polarization values (P_r and P_s) under various poling field strengths are observed, while the coercive field (E_c) remains rather constant. The hysteresis parameter data as a function of poling field strength are summarized in Table 4.3 for comparison.

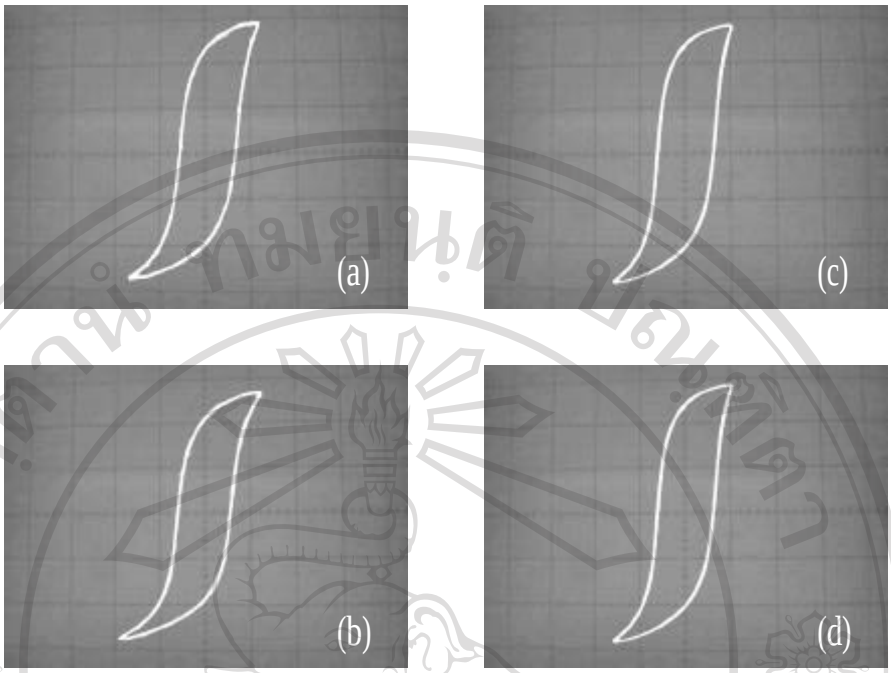

Figure 4.24 The saturated hysteresis loop of 0.1PMN-0.9PZT ceramic poled at poling field strength of: (a) 10, (b) 20, (c) 30 and (d) 40 kV/cm

Table 4.3 Remanent polarization (P_r), spontaneous polarization (P_s) and coercive field (E_c) of 0.1PMN-0.9PZT ceramic

Poling field strength	P_r ($\mu C/cm^2$)	P_s ($\mu C/cm^2$)	E_c (kV/cm)
10 kV/cm	13.16	18.95	5.48
20 kV/cm	18.09	22.21	5.48
30 kV/cm	18.91	23.03	5.48
40 kV/cm	19.74	23.03	5.48

Apparently, both of the polarization (P_r and P_s) increase non-linearly with the increment of the poling field strength. It can be seen that the values of polarization increase largely during initial poling field strength (10-20 kV/cm), and then eventually increase only slightly (or even stable for the spontaneous polarization) with further increase of the poling field strength to 30 and 40 kV/cm. These results are due to existence of macrodomains and microdomains. At low poling field strength of 10 kV/cm, this magnitude of poling field does not provide enough energy to

switch macrodomains but provides just enough for microdomain switching. Whereas, the higher poling field strength of 20 kV/cm, the energy is enough to switch both macrodomains and microdomains. Therefore, large changes of the polarization values occur between poling field strength of 10 and 20 kV/cm. On the other hand, the coercive field (E_c) is relatively stable with increment of the poling field strength. The reason for this observation is not clearly understood, but could probably due to the unstability of these domains as well as the intrinsic nature of the coecive field. The variations of hysteresis parameters as a function of the poling field strength is clearly illustrated in figure 4.25.

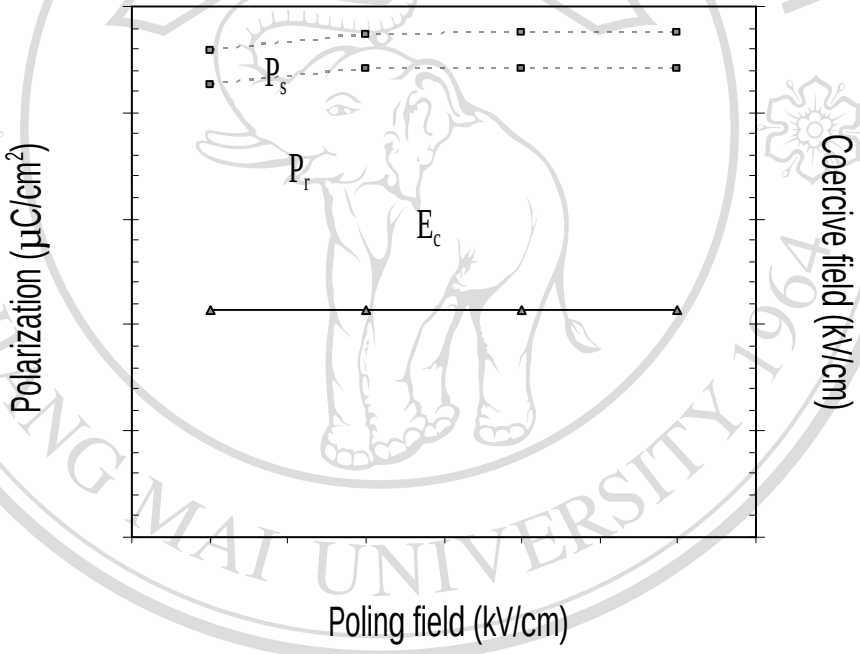

Figure 4.25 The remanent polarization (P_r), spontaneous polarization (P_s) and coercive field (E_c) of 0.1PMN-0.9PZT ceramic as a function of poling field strength

4.4.2.3. 0.3PMN-0.7PZT

In case of 0.3PMN-0.7PZT composition, the series hysteresis loops as function of different poling field strengths between 10 and 40 kV/cm are depicted in figure 4.26. Similar to the results of the 0.1PMN-0.9PZT composition, the hysteresis loop shapes are fairly stable with poling field strength. It is noticeable that the stable shape of hysteresis loops appears for (x)PMN-(1-x)PZT ceramic containing PMN. At poling field strength of 10 kV/cm, it can be said that there is enough energy to switch almost all macrodomains. Therefore, at the higher poling field strength, extra

energy only moves a small amount of the remaining microdomains to follow to electric field direction. Therefore, only very slight increase in the hysteresis parameters with the poling field strength is expected, as shown in Table 4.4.

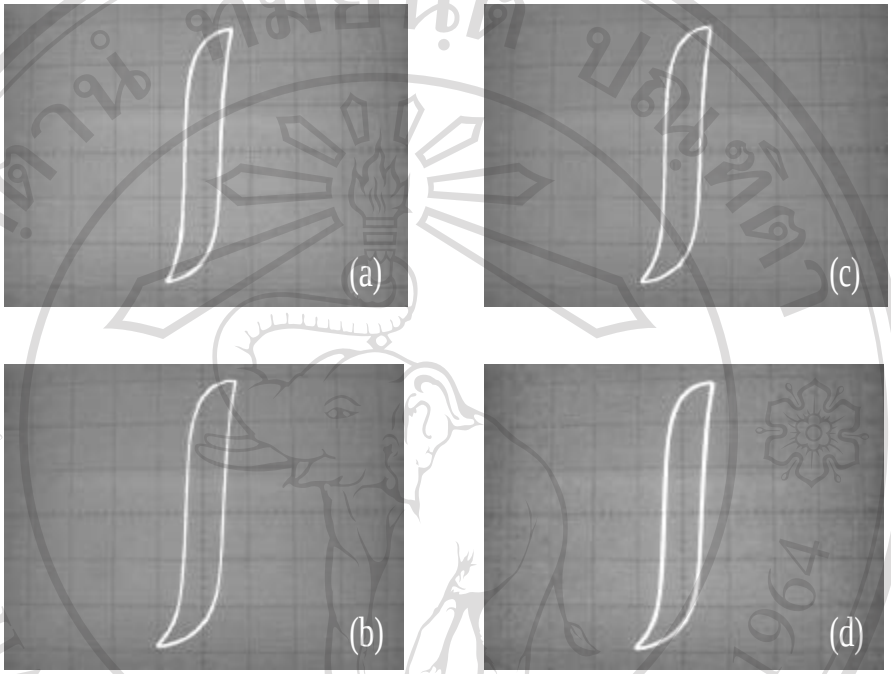

Figure 4.26 The saturated hysteresis loops of 0.3PMN-0.7PZT ceramics poled at poling field strength of: (a) 10, (b) 20, (c) 30 and (d) 40 kV/cm

Table 4.4 Remanent polarization (P_r), spontaneous polarization (P_s) and coercive field (E_c) of 0.3PMN-0.7PZT ceramic

Poling field strength	P_r ($\mu C/cm^2$)	P_s ($\mu C/cm^2$)	E_c (kV/cm)
10 kV/cm	21.26	22.96	4.29
20 kV/cm	22.11	23.66	4.29
30 kV/cm	22.11	23.81	4.29
40 kV/cm	22.11	23.81	4.29

Figure 4.27 also demonstrates that the polarization values change very slightly at initial increase of the poling field strength (10-20 kV/cm), then the values become constant. This observation is rather similar to the case of 0.1PMN-0.9PZT composition. Similar result is also obtained for the coercive field.

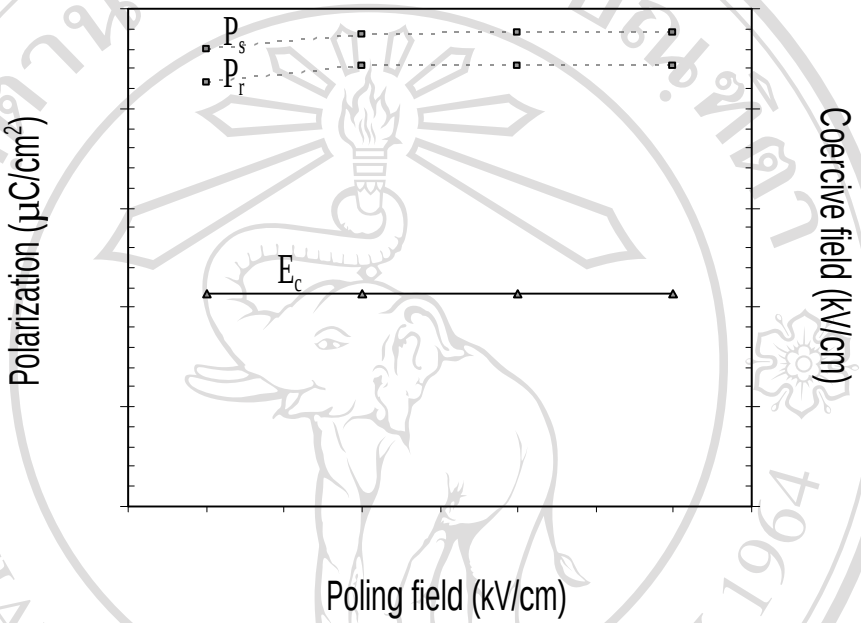

Figure 4.27 The remanent polarization (P_r), spontaneous polarization (P_s) and coercive field (E_c) of 0.3PMN-0.7PZT ceramic as a function of poling field strength

4.4.2.4. 0.5PMN-0.5PZT

The series of hysteresis loops at differnt poling field strength for 0.5PMBN-0.5PZT are illustrated in figure 4.28. Generally, the hysteresis loop shape does not vary with poling field. Therfore, the polarizations (P_r and P_s) and the coercive field do not vary much with poling field strength. The hysteresis parameters are listed in Table 4.5.

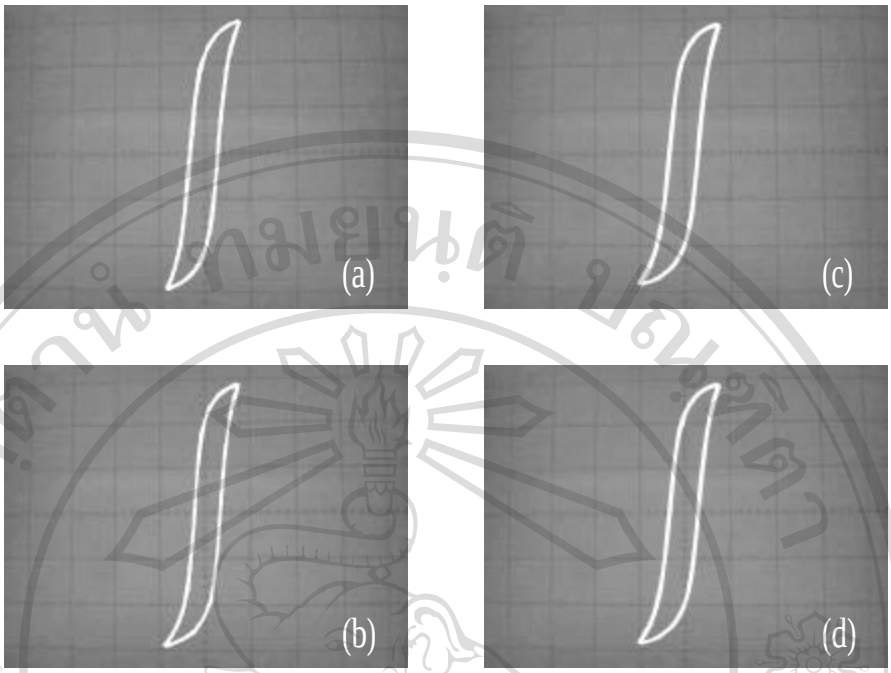

Figure 4.28 The saturated hysteresis loop of 0.5PMN-0.5PZT ceramic poled at poling field strength of: (a) 10, (b) 20, (c) 30 and (d) 40 kV/cm

Table 4.5 Remanent polarization (P_r), spontaneous polarization (P_s) and coercive field (E_c) of 0.5PMN-0.5PZT ceramic

Poling field strength	P_r ($\mu C/cm^2$)	P_s ($\mu C/cm^2$)	E_c (kV/cm)
10 kV/cm	18.10	21.76	4.34
20 kV/cm	19.26	22.61	4.34
30 kV/cm	19.26	22.61	4.34
40 kV/cm	19.26	22.61	4.34

Clearly, these results are similar to the other compositions described earlier in which the polarization values (P_r and P_s) increase during initial increase of poling field strength, then the values become constant with further increase of poling field strength to 40 kV/cm, while the coercive field (E_c) is very stable despite an increase in the poling field strength field, as shown clearly in figure 4.29.

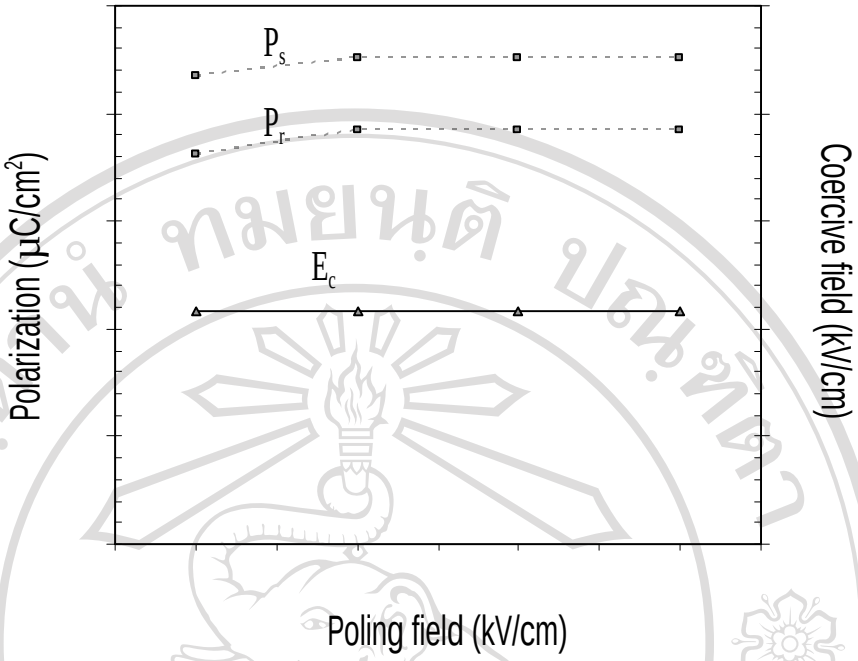

Figure 4.29 The remanent polarization (P_r), spontaneous polarization (P_s) and coercive field (E_c) of 0.5PMN-0.5PZT ceramic as a function of poling field strength

4.4.2.5. 0.7PMN-0.3PZT

In this PMN-riched composition, hysteresis with slim loop shapes is obtained. As shown in figure 4.30, the shapes of the hysteresis loop do not change with increment of poling field strength. This shows that increasing PMN content results in decreasing of macrodomains. Therefore, the poling field of 10 kV/cm is expected to give enough energy to induce switching of almost all the macrodomains to poling field direction. Moreover, the hysteresis parameters change with the poling field strength in a similar manner to the previously described compositions, in which the polarization values alter while coercive field does not change with increment of poling field. The results of determined parameters are summarized in Table 4.6.

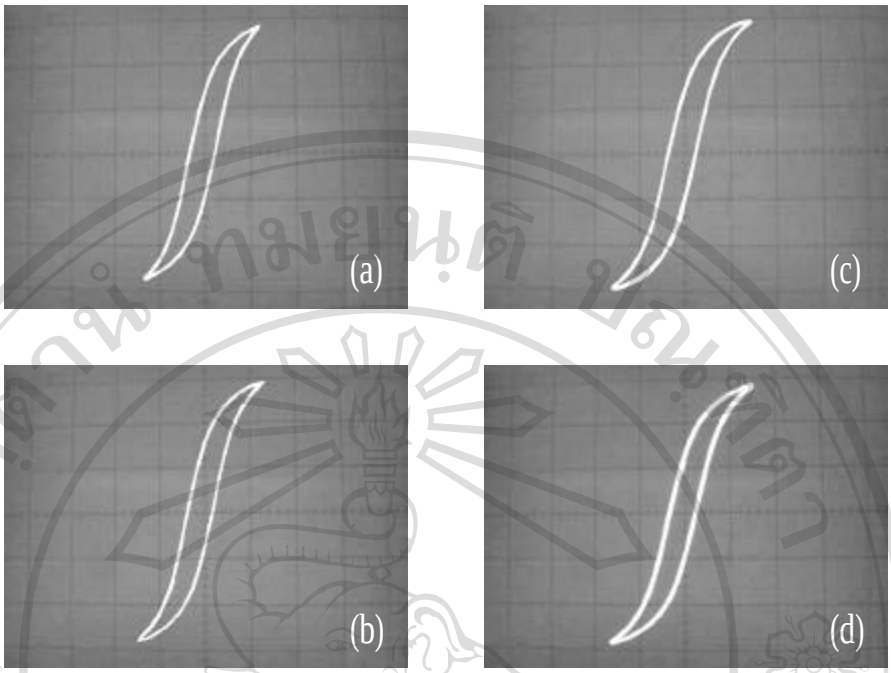

Figure 4.30 The saturated hysteresis loops of 0.7PMN-0.3PZT ceramic pled at poling field strength of: (a) 10, (b) 20, (c) 30 and (d) 40 kV/cm

Table 4.6 Remanent polarization (P_r), spontaneous polarization (P_s) and coercive field (E_c) of 0.7PMN-0.3PZT ceramic

Poling field strength	P_r ($\mu C/cm^2$)	P_s ($\mu C/cm^2$)	E_c (kV/cm)
10 kV/cm	10.38	18.83	2.38
20 kV/cm	11.98	20.54	2.38
30 kV/cm	11.98	20.54	2.38
40 kV/cm	11.98	20.54	2.38

Once again, this table shows clearly that the polarizations increase during initial poling field strength, and then become constant, whereas coercive field is always constant. Figure 4.31 also depicts the changes.

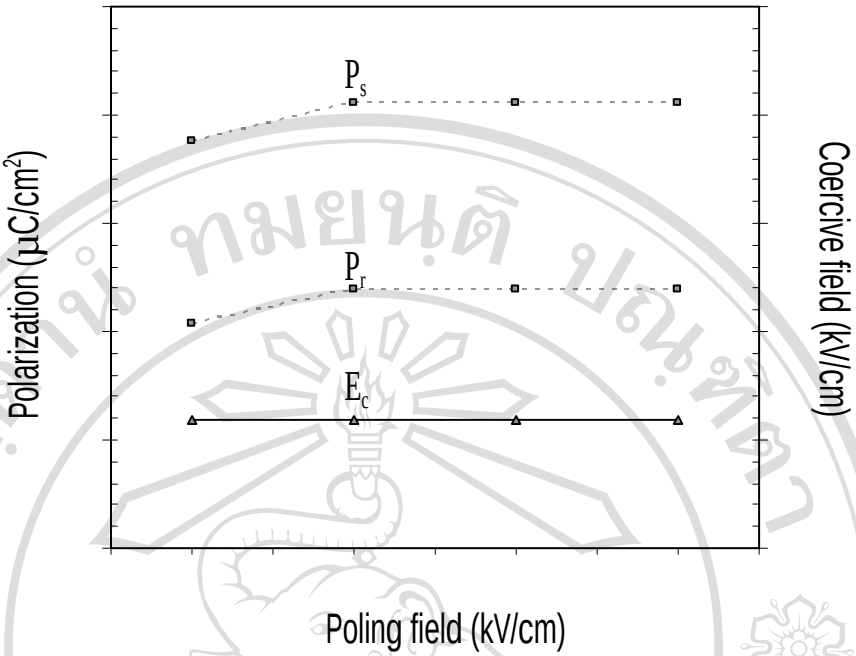

Figure 4.31 The remanent polarization (P_r), spontaneous polarization (P_s) and coercive field (E_c) of 0.7PMN-0.3PZT ceramic as a function of poling field strength

4.4.2.6. 0.9PMN-0.1PZT

In this ceramic which a large portion of PMN, it shows the hysteresis properties similar to those of pure PMN ceramic, which exhibits the slim loop at room temperature. Therefore, the hysteresis loop shapes are fairly stable as shown in figure 4.32. However, the slight change is observed for hysteresis parameters such as the polarizations. Table 4.7 shows the hysteresis parameters at different poling field strength. It can be seen that the polarization values increase slightly at the initial poling field strength before becoming constant, while the coercive field remains constant throughout. Clearer comparison of the hysteresis parameters is illustrated in figure 4.33. Generally, the hysteresis parameters are relatively stable.

Table 4.7 Remanent polarization (P_r), spontaneous polarization (P_s) and coercive field (E_c) of 0.9PMN-0.1PZT ceramic

Poling field strength	P_r ($\mu C/cm^2$)	P_s ($\mu C/cm^2$)	E_c (kV/cm)
10 kV/cm	4.23	16.07	0.96
20 kV/cm	5.08	16.46	0.96
30 kV/cm	5.08	16.92	0.96
40 kV/cm	5.05	16.92	0.96

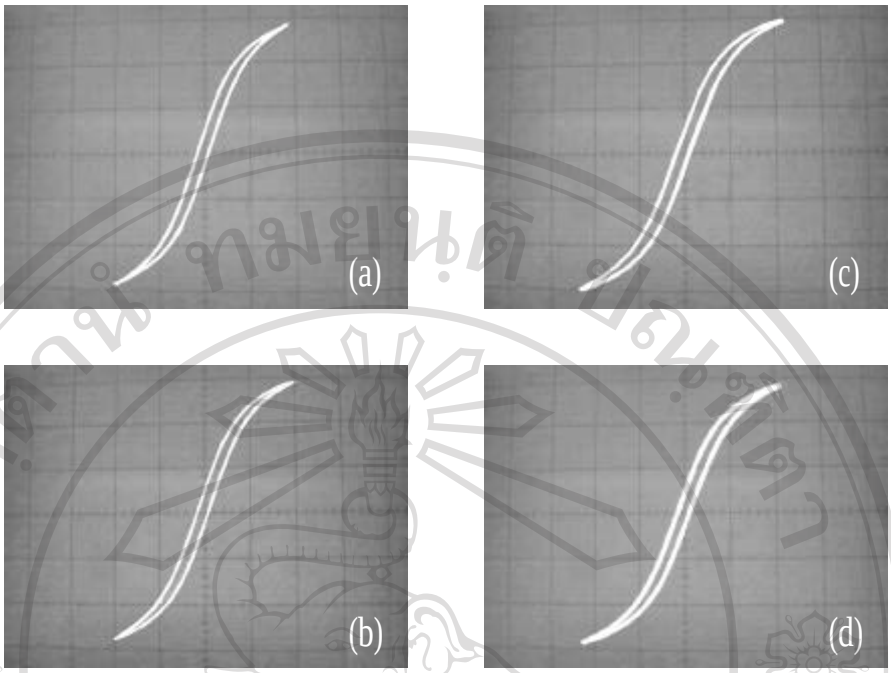

Figure 4.32 The saturated hysteresis loop of 0.9PMN-0.1PZT ceramic poled at poling field strength of: (a) 10, (b) 20, (c) 30 and (d) 40 kV/cm

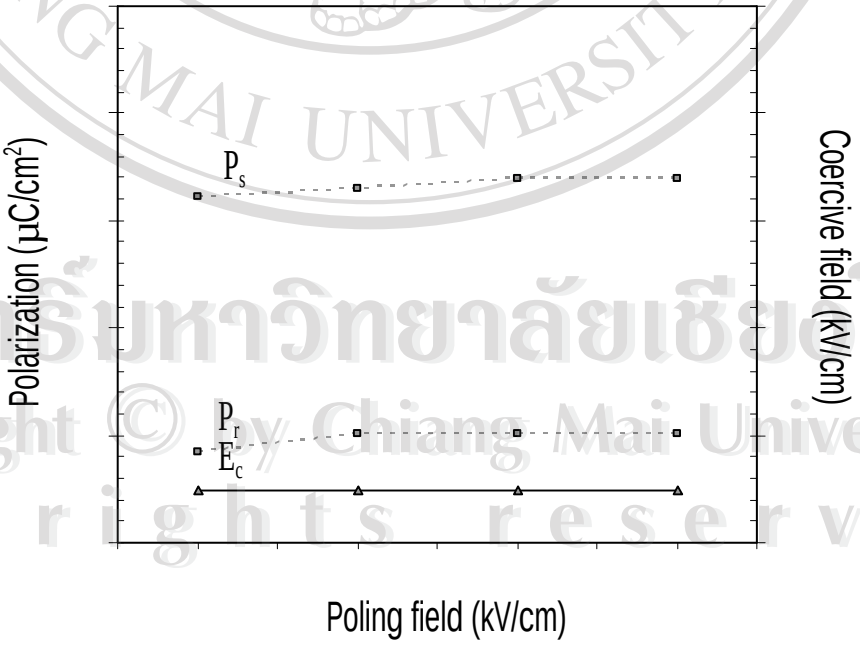

Figure 4.33 The remanent polarization (P_r), spontaneous polarization (P_s) and coercive field (E_c) of 0.9PMN-0.1PZT ceramic as a function of poling field strength

4.4.2.7. PMN

In pure PMN, the slim loop hysteresis can be obtained, as a result of the existence of almost all microdomains (or nano-polar regions) at room temperture. Therefore, the changes of hysteresis properties are affected by the change of microdomains under an electric field. Figure 4.34 shows the series of slim hysteresis loops for PMN at various poling field strengths. Generally, the shape of the loop is very similar. However, slight changes of the polarization values with poling field strength are observed. The determined hysteresis parameters are listed in Table 4.8.

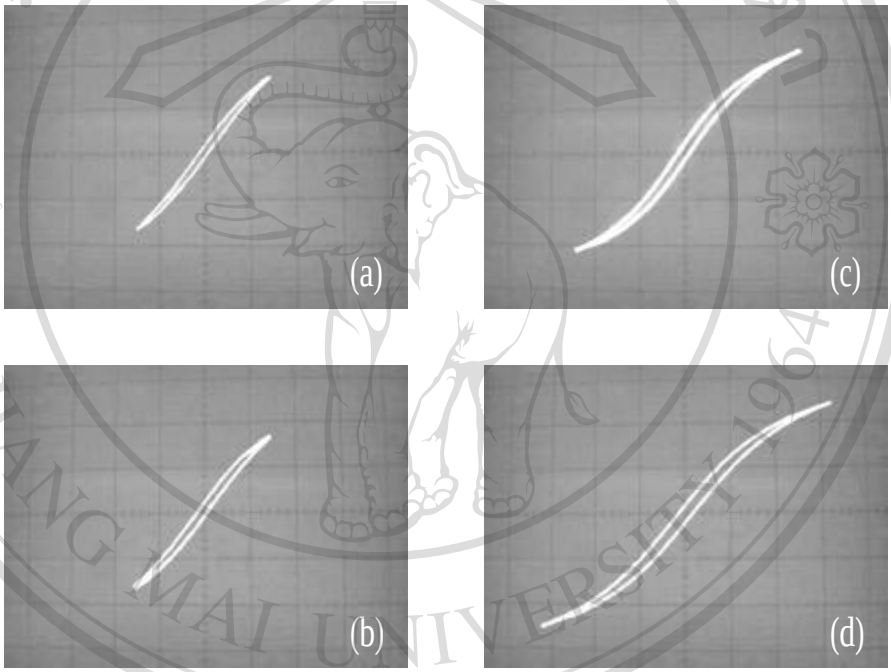

Figure 4.34 The saturated hysteresis loop of PMN ceramic poled at poling field strength of: (a) 10, (b) 20, (c) 30 and (d) 40 kV/cm

Table 4.8 Remanent polarization (P_r), spontaneous polarization (P_s) and coercive field (E_c) of PMN ceramic

Poling field strength	P_r ($\mu C/cm^2$)	P_s ($\mu C/cm^2$)	E_c (kV/cm)
10 kV/cm	1.27	4.88	0.78
20 kV/cm	1.63	9.76	0.78
30 kV/cm	1.63	8.13	0.78
40 kV/cm	1.63	10.57	0.78

Table 4.8 shows that the remanent polarization increase during an initial increase of poling field strength from 10 to 20 kV/cm, then the value becomes constant. Whereas, the spontaneous polarization increases continuously with increasing poling field strength. This confirms that the sintered PMN ceramic which is polycrystalline needs to be poled to determine dominant paraelectric properties. On the other hand, coercive field remains constant. Clear comparison of hysteresis parameters is shown in figure 4.35.

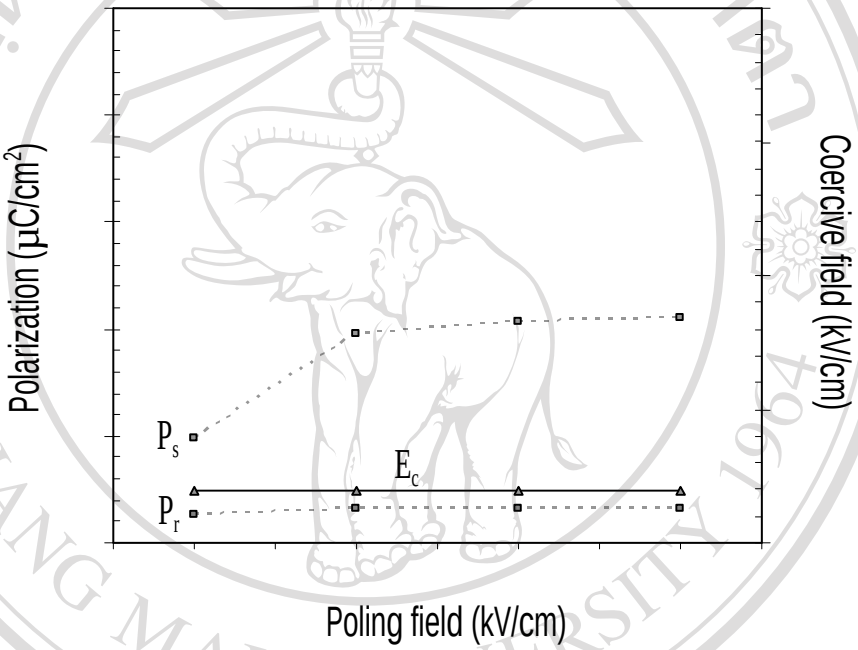

Figure 4.35 The remanent polarization (P_r), spontaneous polarization (P_s) and coercive field (E_c) of 0.7PMN-0.3PZT ceramic as function of poling field strength

Finally, the results on the effect of poling field strength on the hysteresis properties of PMN-PZT ceramics are summarized in the following ways. It is clear that the poling field strength has little effect on hysteresis parameters of PMN-riched compositions (when $0.5 \leq x \leq 1$) but shows marked effect on those of PZT-riched compositions (when $0 \leq x \leq 0.3$). The polarization (P_r and P_s) and coercive field (E_c) of PZT ceramic are largely increased with increasing of poling field strength, while the values of polarization (P_r and P_s) ceramic compositions with $x = 0.1$ and $x = 0.3$ are slightly increased but E_c remains constant. These results are due to a characteristic of PZT ceramics with composition near the morphotropic phase boundary (MPB) between the rhombohedral and the tetragonal phases in which the poling may

draw upon 14 orientation states leading to exception polability. Therefore, they are easier to pole than PMN ceramic.[1] The results of ceramic with x = 0.1 and x = 0.3 are due to coexistent of dominant phase of PZT and inferior psudocubic PMN phase. On the other hand, polarizations (P_r and P_s) of PMN-riched compositions are increased until poling field strength reaches 20 kV/cm, then become constant with further increasing of the poling field strength, while E_c remains unchanged. These results are probably due to the fact that the poling field strength of 20 kV/cm provides enough energy to constrain all macrodomains and microdomains switching under a DC field direction. Generally, the hysteresis parameters, the polarizations (P_r and P_s) and coercive field of (x)PMN-(1-x)PZT ceramics are increased with increasing the poling field strength, with maximum values of hysteresis parameters at the poling field of 30 kV/cm, which corresponds to other research.[8] This result indicates that the poling field strength of 30 kV/cm provides enough energy to switch both macrodomains and microdomains direction to the applied field direction.

4.4.3. Hysteresis properties dependence on composition ratio

The room temperature hysteresis (P vs E) nature of each composition of (x)PMN-(1-x)PZT ceramics was investigated by applying AC electric field until saturated loop occurs. The P-E loop of this system is shown in previous section. In this section, the remanent polarization (P_r), spontaneous polarization (P_s) and coercive field (E_c) are determined as a function of the composition. The determined hysteresis parameters of saturated loop are presented for several (x)PMN-(1-x)PZT compositions. In general, the magnitudes of the polarization (P_r and P_s) and coercive field (E_c) were found to vary with PMN content. In this section, the results are described for each poling field strength.

4.4.3.1. The remanent polarization (P_r), spontaneous polarization (P_s) and coercive field (E_c) of (x)PMN-(1-x)PZT poled at 10 kV/cm

At 10 kV/cm poling field strength, it seems there is not enough energy to switch domains to follow the electric field direction. Therefore, the results show that the applied field affects only few domains, especially in PZT. The determined hysteresis parameters are listed in Table 4.9. It is seen that the polarizations (P_r and P_s) of the ceramics show maximum values (of 21.26 $\mu C/cm^2$ and 22.96 $\mu C/cm^2$, respectively) at the composition with x = 0.3.

Table 4.9 Remanent polarization (P_r), spontaneous polarization (P_s) and coercive field (E_c) of PMN-PZT ceramics poled at 10 kV/cm

composition	P_r ($\mu C/cm^2$)	P_s ($\mu C/cm^2$)	E_c (kV/cm)
PZT	0.82	1.68	0.79
0.1PMN-0.9PZT	13.16	18.95	5.48
0.3PMN-0.7PZT	21.26	22.96	4.29
0.5PMN-0.5PZT	18.10	21.76	4.34
0.7PMN-0.3PZT	10.38	18.83	2.38
0.9PMN-0.1PZT	4.23	16.07	0.96
PMN	1.27	4.88	0.78

It should be noted, comparing the values of remanent polarization for all studied ferroelectric samples, that the remanent polarization of the composition with x = 0.3 near the MPB (morphotropic phase boundary) is largest (as seen in figure 4.35). It is well known that the polarization vector of the coexistence phases has more possible directions for dipole moment reorientation. In addition, the existence of a pseudocubic phase in (x)PMN-(1-x)PZT (when $0.3 < x < 1$) reduces significantly the remanent polarization of ferroelectrics. However, the maximum value of coercive field (E_c) of 5.48 kV/cm is observed for the composition with x = 0.1. Moreover, it can noticed that the coercive field for $0.1 \leq x \leq 0.5$ compositions is larger than that of other compositions, probably due to the significant reduction of the remanent polarization. From the above results, as expected, the ceramic composition with x = 0.3, which lies near the MPB, shows enhanced hysteresis properties. Furthermore, the larger value of coercive field of ceramic compositions with x = 0.1, 0.3 and 0.5 also shows a strong correlation with remanent and spontaneous polarizations.

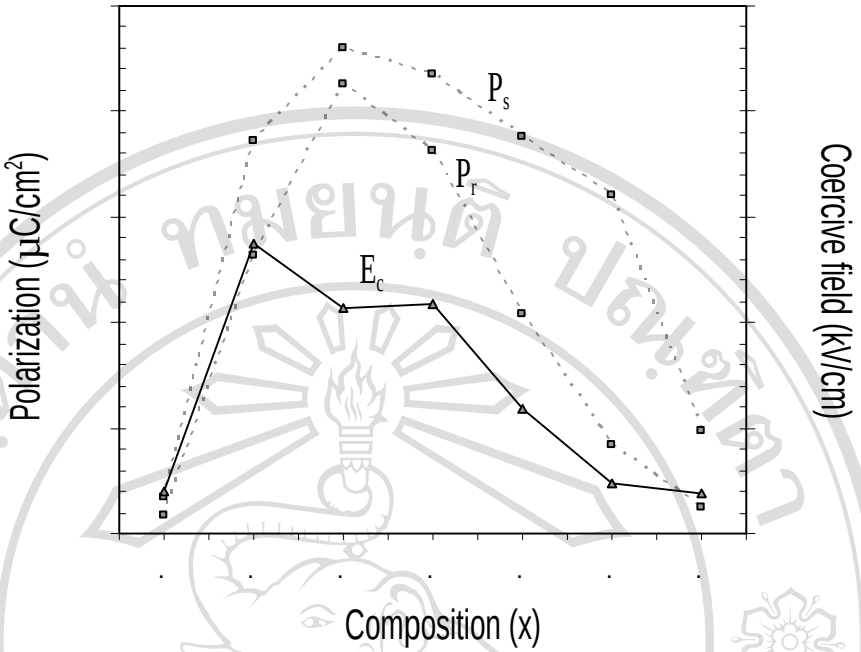

Figure 4.36 The remanent polarization (P_r), spontaneous polarization (P_s) and coercive field (E_c) of (x)PMN-(1-x)PZT ceramics poled at 10 kV/cm

4.4.3.2. The remanent polarization (P_r), spontaneous polarization (P_s) and coercive field (E_c) of (x)PMN-(1-x)PZT poled at 20 kV/cm

At 20 kV/cm poling field strength, there seems to be enough energy to move domains to the direction of electric field. This is evident from the noticeable increase of polarization values. The data of hysteresis parameters are listed in Table 4.10. It is found that the maximum values of polarizations (P_r and P_s) are similar to those of the ceramics poled at 10 kV/cm. The peak values of remanent polarization and spontaneous polarization are found to be about 22.11 $\mu C/cm^2$ and 22.96 $\mu C/cm^2$ for ceramic composition with x = 0.3, respectively. These results are the influence of near MPB composition of PMN-PZT system. In addition, the maximum coercive field of 5.48 kV/cm is still observed at x = 0.1 composition.

Better comparisons of the hysteresis parameters are shown in figure 4.34. The results do not follow the same trend as in the 10 kV/cm poling field. In this case, the coercive field does not follow the remanent polarization values, in particular for PZT ceramics, due to the asymmetric loop of PZT ceramic. Furthermore, the high coercive fields observed for $0.1 \leq x \leq 0.5$ compositions imply strong induce of the polarization.

Table 4.10 Remanent polarization (P_r), spontaneous polarization (P_s) and coercive field (E_c) of PMN-PZT ceramics poled at 20 kV/cm

composition	P_r ($\mu C/cm^2$)	P_s ($\mu C/cm^2$)	E_c (kV/cm)
PZT	0.00	2.53	4.77
0.1PMN-0.9PZT	18.09	22.21	5.48
0.3PMN-0.7PZT	22.11	23.66	4.29
0.5PMN-0.5PZT	19.26	22.61	4.34
0.7PMN-0.3PZT	11.98	20.54	2.38
0.9PMN-0.1PZT	5.06	16.46	0.96
PMN	1.63	9.76	0.78

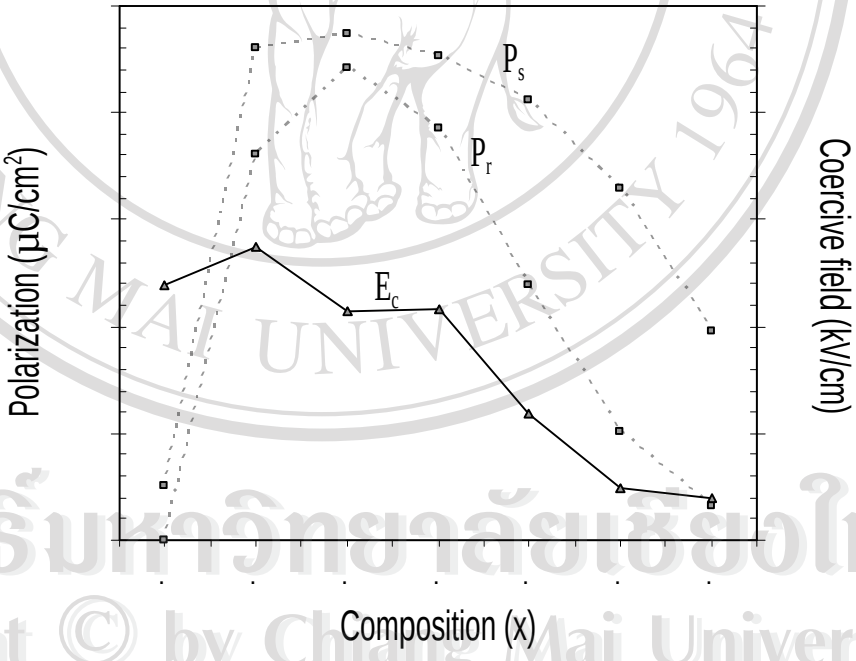

Figure 4.37 The remanent polarization (P_r), spontaneous polarization (P_s) and coercive field (E_c) of (x)PMN-(1-x)PZT ceramics poled at 20 kV/cm

4.4.3.3. The remanent polarization (P_r), spontaneous polarization (P_s) and coercive field (E_c) of (x)PMN-(1-x)PZT poled at 30 kV/cm

In this case, it is clearly evident that the poling field strength strongly affects the hysteresis properties of PZT ceramic. This is probably due to macrodomain response to the applied field in PZT ceramics. The hysteresis parameters are listed in Table 4.11. It is clear that the polarizations tend to increase until reaching peak values at x = 0.3 composition, then decrease for higher PMN content. The remanent and spontaneous polarizations of 22.11 $\mu C/cm^2$ and 23.81 $\mu C/cm^2$, respectively, are found in ceramics with x = 0.3 as a result of MPB near this compostion. On the other hand, it is found that the maximum value of 7.95 kV/cm for coercive field is observed in PZT ceramic, and then the values continuously decrease with higher PMN content. It implies that PZT (E_c = 7.95 kV/cm) is more easily induced under electric field than that other MPB compositions (E_c = 4.29-5.48 kV/cm) which contain a large amount of the psudocubic PMN phase.

Table 4.11 Remanent polarization (P_r), spontaneous polarization (P_s) and coercive field (E_c) of PMN-PZT ceramics poled at 30 kV/cm

composition	P_r ($\mu C/cm^2$)	P_s ($\mu C/cm^2$)	E_c (kV/cm)
PZT	10.10	23.58	7.95
0.1PMN-0.9PZT	18.91	23.03	5.48
0.3PMN-0.7PZT	22.11	23.81	4.29
0.5PMN-0.5PZT	19.26	22.61	4.34
0.7PMN-0.3PZT	11.98	20.54	2.38
0.9PMN-0.1PZT	5.08	16.92	0.96
PMN	1.63	8.13	0.78

Clearer comparison of the hysteresis parameters is plotted in figure 4.35. It can be seen that the remanent polarization of 10.10 $\mu C/cm^2$ is observed for composition with the maximum coercive field (PZT). This observation disagrees with the results from previous sections, in which the maximum value of the coercive field usually corresponds to the maximum values of remanent polarization. It is in part due to pinning effect (such as porosity, defect) which suppresses domain motion in PZT.[62]

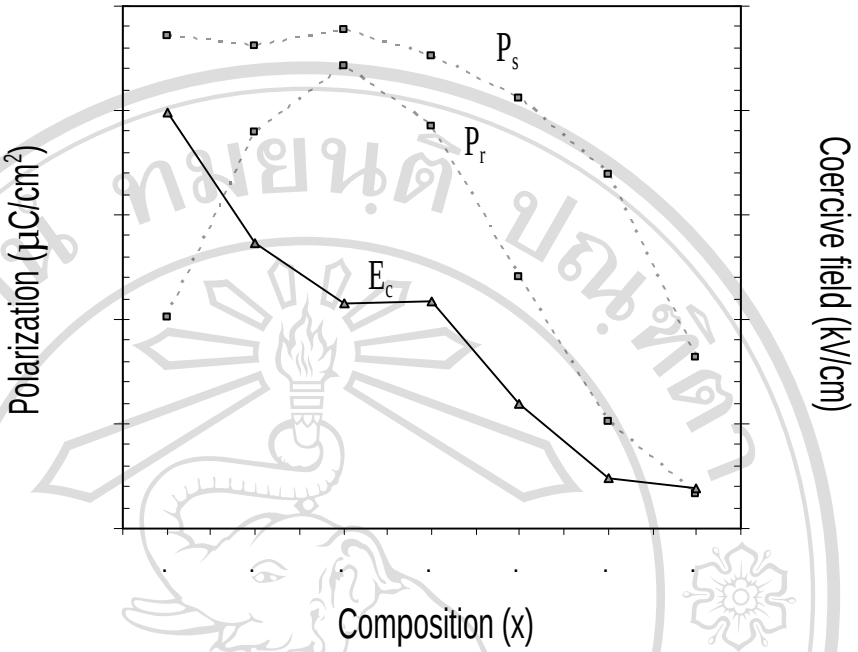

Figure 4.38 The remanent polarization (P_r), spontaneous polarization (P_s) and coercive field (E_c) of (x)PMN-(1-x)PZT ceramics poled at 30 kV/cm

4.4.3.4. The remanent polarization (P_r), spontaneous polarization (P_s) and coercive field (E_c) of (x)PMN-(1-x)PZT poled at 40 kV/cm

At 40 kV/cm of poling field strength, only the hysteresis parameters of (x)PMN-(1-x)PZT ceramics with $0.1 \leq x \leq 1.0$ are obtained because breakdown occurred in PZT ceramic at in this poling condition. The hysteresis parameters of other compositions are shown in Table 4.12. It can be observed that the polarizations increase to the peak values at x = 0.3, then decrease continuously with higher PMN contents. Moreover, it is found that the coercive field decreases with increasing PMN content. These results are similar to ceramics poled at 30 kV/cm. It can be seen from figure 4.39 that the hysteresis parameters (P_s, P_s and E_c) decrease with increasing the content of PMN into the (x)PMN-(1-x)PZT composition (when $x = 0.3$). This indicates that the hysteresis parameters are lowered as a result of PMN addition. This can be understood from the fact that PMN itself is transforming into a paraelectric (non-hysteretic) phase at temperature above its Curies temperature ~ -10 °C, and all the measurements done here are carried out at room temperature of 30°C or more.

Table 4.12 Remanent polarization (P_r), spontaneous polarization (P_s) and coercive field (E_c) of PMN-PZT ceramics poled at 40 kV/cm

composition	P_r ($\mu C/cm^2$)	P_s ($\mu C/cm^2$)	E_c (kV/cm)
PZT	Break down	Break down	Break down
0.1PMN-0.9PZT	19.74	23.03	5.48
0.3PMN-0.7PZT	22.11	23.81	4.29
0.5PMN-0.5PZT	19.26	22.61	4.34
0.7PMN-0.3PZT	11.98	20.54	2.38
0.9PMN-0.1PZT	5.08	16.92	0.96
PMN	1.63	10.57	0.78

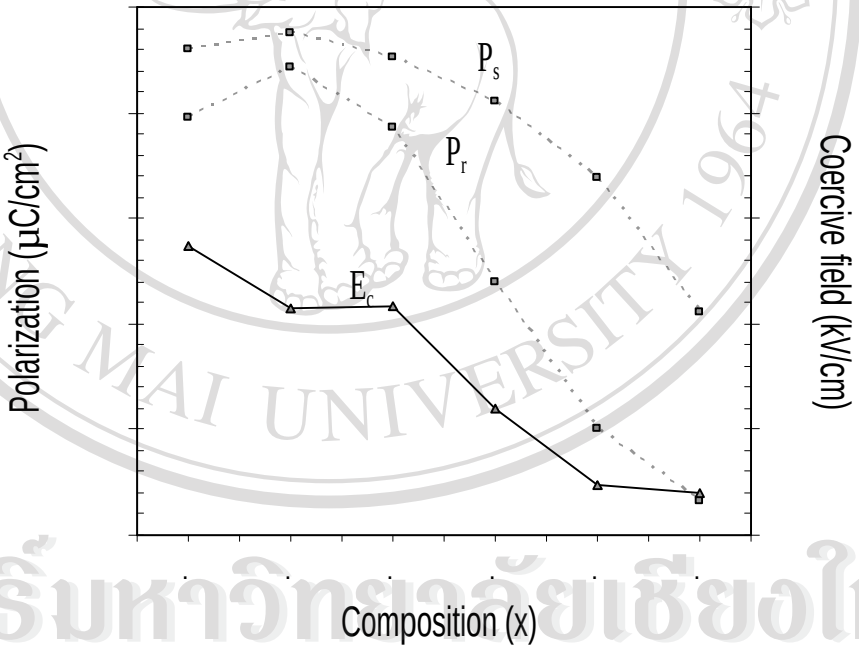

Figure 4.39 The remanent polarization (P_r), spontaneous polarization (P_s) and coercive field (E_c) of (x)PMN-(1-x)PZT ceramic which poled at 40 kV/cm

In conclusion, this section describes the hysteresis parameters as a function ofcomposition ratio. The results indicate the maximum values of polarizations (P_r and P_s) at the 0.3PMN-0.7PZT ceramic for every poling field strength and the results of XRD analysis which show the significant change of XRD pattern at the composition between of x = 0.3 and x = 0.5. This implies this the ceramic composition between of x = 0.3 and x = 0.5 lies near the MPB of the

PMN-PZT ceramic system.[8] It may be the reason that the phase coexistence offers more polarization at phase boundary.[68] In addition, the decrease of polarizations for compositions with $x > 0.3$ with increment of PMN content, is in part due to PMN itself is transforming into a paraelectric (non-hysteresis) phase at temperature above ~ -10 °C.[12] Furthermore, the coercive field shows the maximum value for PZT and decreases with increment of PMN contents. This agrees with the work by Benguigui[69] in which Laudau-Devonshire theory[70] was used to explain the phenomenon. The tetragonal phase obviously has a higher E_c than the psudocubic phase. The coercive field is nearly constant for the psudocubic composition, but increases with increasing PZT in the tetragonal region.

4.4.4. The maximum hysteresis parameters for PMN-PZT ceramics

The hysteresis parameters as function of poling field and composition were described in the previous section, the maximum values of these parameters for each composition are shown in Table 4.13. Generally, the maximum values of the hysteresis parameters (P_r, P_s and E_c) are obtained at 30 kV/cm poling field strength. At any poling condition, the polarizations (P_r and P_s) data show peak values at $x = 0.3$, owning to these compositions close to the MPB of PMN-PZT system.[8] It could be speculated that MPB of (x)PMN-(1-x)PZT lies compositions with $x = 0.3$. On the other hand, the maximum coercive field is determined in PZT ceramic.

Table 4.13 The maximum value of remanent polarization (P_r), spontaneous polarization (P_s) and coercive field (E_c) of PMN-PZT ceramics

composition	$P_{r,\,max}$ ($\mu C/cm^2$)	$P_{s,\,max}$ ($\mu C/cm^2$)	$E_{c,\,max}$ (kV/cm)
PZT	10.10	23.58	7.95
0.1PMN-0.9PZT	19.74	23.03	5.48
0.3PMN-0.7PZT	22.11	23.81	4.29
0.5PMN-0.5PZT	19.26	22.61	4.34
0.7PMN-0.3PZT	11.98	20.54	2.38
0.9PMN-0.1PZT	5.08	16.92	0.96
PMN	1.63	10.57	0.78